ALTERNATIVE MATCHING SCHEMES FOR AUTOMATIC FINGERPRINT IDENTIFICATION SYSTEMS

by

MICHAEL JASON FUTER

Presented to the Faculty of the Graduate School of

The University of Texas at Arlington in Partial Fulfillment

of the Requirements

for the Degree of

MASTER OF SCIENCE IN ELECTRICAL ENGINEERING

THE UNIVERSITY OF TEXAS AT ARLINGTON

December 2010

ACKNOWLEDGEMENTS

I wish to thank Dr. Michael Manry for serving as my Master's Thesis advisor during my final semesters as a student at The University of Texas at Arlington. His technical guidance, encouragement, patience and understanding have proven invaluable throughout the many challenges of completing a Master's Thesis research project. I especially appreciate his willingness to allow me to complete my research on a part-time basis, as this was necessary for me while employed as a full time electrical engineer in the U.S. government defense industry in addition to attending graduate school.

I would also like to thank Dr. K.R. Rao and Dr. Venkat Devarajan for serving alongside Dr. Michael Manry on my M.S. Thesis defense committee. On top of that, I am grateful for the knowledge I obtained from all three professors while I was enrolled in their graduate-level Electrical Engineering courses.

Next, I want to express my deepest gratitude to J. Michael and Carole Futer for being the most supportive, encouraging and selfless parents an engineering graduate student could want. The moral values, desire for financial independence and strong work ethic they taught me since childhood has helped me to succeed in my graduate studies at The University of Texas at Arlington. I certainly would not have made it this far in my education without them.

Finally, I wish to thank my younger brother, Joshua Futer, and all of my friends for respecting the fact that my graduate studies were a higher priority than the social and leisure time activities we enjoy doing together. Their patience and understanding during this time in my life is greatly appreciated.

November 22, 2010

ABSTRACT

ALTERNATIVE MATCHING SCHEMES FOR AUTOMATIC

FINGERPRINT IDENTIFICATION SYSTEMS

Michael Jason Futer, M.S.

The University of Texas at Arlington, 2010

Supervising Professor: Michael T. Manry

Biometrics is a recognition technology that uses the unique behavioral and physiological traits of the human body as identifiers. The fingerprint is one of the oldest and most widely used forms of biometric identifiers. In this thesis, an automatic fingerprint identification system designed by a previous Electrical Engineering graduate student at The University of Texas at Arlington is upgraded with the purpose of improving matching accuracy. A review of the baseline automatic fingerprint identification system is provided as a reference point for improvements in the system. Then, improvements to the image enhancement stage of the baseline system are discussed. They include replacing the simple transformation contrast stretching algorithm with the "contract and stretch" algorithm and upgrading the threshold variance in image segmentation to a threshold variance to mean ratio. Next, improvements to the feature extraction and fusion stage of the baseline system are covered. A new method for quantizing ridge direction estimates in the direction image is included in this section. Finally, alternative matching schemes are implemented in the correlation-based matching stage of the baseline system. The new matching schemes include direction only feature, density only

feature, two channels with addition-type fusion, two channels with multiplication-type fusion and two templates per class. At the end, simulations are performed in order to test the performance of the improvements implemented in the automatic fingerprint identification system.

TABLE OF CONTENTS

ACKNOWLEDGEMENTS iii

ABSTRACT iv

LIST OF ILLUSTRATIONS ix

LIST OF TABLES xi

Chapter Page

1. INTRODUCTION 1

1.1 Conventional Methods of Personal Identification 1

1.2 Biometrics 2

1.3 Fingerprint as a Biometric Identifier 2

1.3.1 History and Human Development 2

1.3.2 Function of an Automatic Identification System 3

1.4 Previous Work 3

1.5 Objectives and Overview 4

2. BASELINE AUTOMATIC FINGERPRINT IDENTIFICATION SYSTEM 6

2.1 Analysis of a Fingerprint 6

2.2 Correlation-based Automatic Fingerprint Identification Systems 7

2.3 Review of the Baseline System 9

2.3.1 Image Enhancement Stage 9

2.3.1.1 Assessing Fingerprint Quality 10

2.3.1.2 Contrast Stretching 12

2.3.1.3 Local Histogram Equalization with Image Segmentation 13

2.3.1.4 Local Normalization 16

2.3.1.5 Image Morphology 18
2.3.1.6 Image Enhancement Results..... 19
2.3.2 Feature Extraction and Fusion Stage 20
2.3.2.1 Fingerprint Representation Overview 21
2.3.2.2 Ridge Direction Representation..... 22
2.3.2.3 Ridge Density Representation 24
2.3.2.4 Direction and Density Images Overview..... 25
2.3.2.5 Image Thresholding 25
2.3.2.6 Features Estimation Using Discrete Fourier Transform Approach 27
2.3.2.7 Direction and Density Image Results..... 31
2.3.2.8 Pseudo Spectrum Fusion 32
2.3.3 Correlation-based Matching Stage 33
2.3.3.1 Fused Features Matching 35
2.3.3.2 Correlation-based Matching Results..... 36
2.3.4 Overall Performance Results 39
3. AREAS FOR IMPROVEMENT 40
3.1 Problems to be Addressed..... 40
3.2 Thesis Goal and Tasks 41
4. IMAGE ENHANCEMENT IMPROVEMENTS 43
4.1 Contrast Stretching 43
4.1.1 Algorithm Description..... 43
4.1.2 Performance Evaluation..... 45
4.2 Image Segmentation..... 46
4.2.1 Algorithm Description..... 46

4.2.2 Performance Evaluation 48
4.3 Image Enhancement Results 49
5. FEATURE EXTRACTION AND FUSION IMPROVEMENTS 51
5.1 Direction Image 51
5.1.1 Algorithm Description 51
5.1.2 Performance Evaluation 53
5.2 Direction Image Results 53
6. ALTERNATIVE CORRELATION-BASED MATCHING SCHEMES 55
6.1 Direction Feature Only Matching 55
6.2 Density Feature Only Matching 56
6.3 Two Channels with Addition-Type Fusion Matching 58
6.4 Two Channels with Multiplication-Type Fusion Matching 60
6.5 Two Templates per Class Matching 62
6.6 Correlation-Based Matching Results 64
7. SIMULATION EXPERIMENT RESULTS 70
7.1 Objectives 70
7.2 Fingerprint Database Descriptions 71
7.3 Experiment Setup 71
7.4 Data Formatting Description 73
7.5 Matching Data Results 73
8. CONCLUSIONS AND FUTURE RESEARCH 85
8.1 Conclusions of this Thesis 85
8.2 Recommended Future Research 86
REFERENCES 88
BIOGRAPHICAL INFORMATION 90

LIST OF ILLUSTRATIONS

Figure Page

2.1 Correlation-based Identification System Block Diagram.... 8

2.2 Four Image Enhancement Steps Block Diagram.... 9

2.3 Examples of Different Quality Fingerprint Images. 11

2.4 Example of Contrast Stretching: Before and After (Baseline). 13

2.5 Single-Point Threshold Variance Location.... 15

2.6 Example of LHE with Image Segmentation: Before and After (Baseline).... 16

2.7 Example of Local Normalization: Before and After (Baseline).... 18

2.8 Example of Morphological Opening: Before and After.... 19

2.9 Four Stages of Image Enhancement Examples (Baseline).... 20

2.10 Vector Field Model. 23

2.11 Orientation Field Model.... 23

2.12 Example of Image Thresholding: Before and After (Baseline). 27

2.13 Sample Patterns with Corresponding Re-Ordered Frequency Spectrums.... 29

2.14 Actual Fingerprint Ridge Patterns with Re-Ordered Frequency Spectrums.... 31

2.15 Direction Image and Density Image Examples (Baseline). 32

2.16 Correlation-based Matching: Exact Same Images. 37

2.17 Correlation-based Matching: Different Images from Same Class. 38

2.18 Correlation-based Matching: Different Images from Different Classes. 38

4.1 Example of Contrast Stretching: Before and After (Improved). 45

4.2 Example of LHE with Image Segmentation: Before and After (Improved). 48

4.3 Four Stages of Image Enhancement Examples (Improved).... 50

5.1 Orientation Field Model (Quantized). 52

5.2 Direction Image Examples (Improved)..... 54

6.1 Single Feature Matching: Exact Same Images..... 65

6.2 Single Feature Matching: Different Images from Same Class..... 65

6.3 Single Feature Matching: Different Images from Different Classes..... 66

6.4 Two Channels Matching: Exact Same Images. 66

6.5 Two Channels Matching: Different Images from Same Class. 67

6.6 Two Channels Matching: Different Images from Different Classes. 67

6.7 Fused Features Matching: Exact Same Images. 68

6.8 Fused Features Matching: Different Images from Same Class. 68

6.9 Fused Features Matching: Different Images from Different Classes. 69

LIST OF TABLES

Table Page

2.1 Overall Matching Performance Results (Baseline) 39

4.1 Matching Results (Contrast Stretching Improved) 46

4.2 Matching Results (Contrast Stretching + Image Segmentation Improved) 49

5.1 Matching Results (Contrast Stretching, Image Seg. + Dir. Image Improved) 53

7.1 Direction Feature Only Matching (Database #1) 75

7.2 Density Feature Only Matching (Database #1) 76

7.3 Two Channels with Addition-Type Fusion Matching (Database #1) 76

7.4 Two Channels with Multiplication-Type Fusion Matching (Database #1) 77

7.5 Pseudo Spectrum Fusion Matching (Database #1) 77

7.6 Two Templates per Class Matching (Database #1) 78

7.7 Direction Feature Only Matching (Database #2) 78

7.8 Density Feature Only Matching (Database #2) 79

7.9 Two Channels with Addition-Type Fusion Matching (Database #2) 79

7.10 Two Channels with Multiplication-Type Fusion Matching (Database #2) 80

7.11 Pseudo Spectrum Fusion Matching (Database #2) 80

7.12 Two Templates per Class Matching (Database #2) 81

7.13 Direction Feature Only Matching (Database #3) 81

7.14 Density Feature Only Matching (Database #3) 82

7.15 Two Channels with Addition-Type Fusion Matching (Database #3) 82

7.16 Two Channels with Multiplication-Type Fusion Matching (Database #3) 83

7.17 Pseudo Spectrum Fusion Matching (Database #3) 83

7.18 Two Templates per Class Matching (Database #3)..... 84

7.19 Overall Matching Performance Results (Improved)..... 84

CHAPTER 1

INTRODUCTION

The need for personal identification has grown in recent years due in part to an increase in Internet commerce, a greater use of secured data and more stringent passport controls [1]. It has become a necessity in the Information Age, also referred to as the Information Era, where someone can transfer information easily and have the ability to obtain knowledge in seconds that was once difficult or not possible to find [2].

1.1 Conventional Methods of Personal Identification

One way to establish the identification of a person is via an automatic identification system, which exists in two conventional forms:

1. Knowledge-based and
2. Possession-based (or token-based)

Knowledge-based systems consist of personal identification numbers (PINs) and passwords that are used as identifiers. Possession-based (or token-based) systems include ID cards, Smart cards and keys for identifiers [1], [3], [4].

Though these conventional forms of automatic identification are widely used in society today, they pose a number of risks to personal security. Risks that are encountered when using knowledge-based systems are complicated PINs and passwords can be forgotten by the intended user or less-complex ones can be guessed/hacked by someone who is unauthorized. Possession-based (or token-based) systems run the risk of having cards or keys misplaced, easily forged, lost or stolen. Cards and keys are also difficult to manage in large quantities [3], [4], [5]. A more

advanced automatic identification system that exists today is a form called biometrics, which is also referred to as being-based [4].

1.2 Biometrics

Biometrics is an automatic identification system which uses the unique physiological or behavioral characteristics of the human body as identifiers [1], [3], [5]. In order for a characteristic to qualify as a biometric identifier, it must be:

1. Present in all humans (universal),
2. Different from person to person (unique),
3. Unchanged on an individual's body throughout an entire lifetime (permanent) and
4. Able to be quantitatively measured (collectable) [6], [7]

This identification system is superior to conventional forms because it uses what the person is and not what the person knows or carries [5]. This eliminates the concerns with conventional identification systems where identifiers can be misplaced, easily forged, lost, stolen, forgotten or hacked [3], [4], [5]. Commonly used biometrics identification systems in existence today utilize unique characteristics of the face, fingerprint, iris, retina, voice, palmprint, hand, ear and gait [8].

1.3 Fingerprint as a Biometric Identifier

The fingerprint is the biometric identifier that is studied in this thesis. Details about the history, human development and the function of an automatic identification system are provided in the following sub-sections.

1.3.1 History and Human Development

The fingerprint is one of the oldest and most unique forms of biometric identifiers from person to person. Its origins as a biometric identifier can be found as early as 2200 BC where the Assyrians, Babylonians, Chinese and Japanese used it as a personal code

[9]. In modern times, it has been used in non-computer based identification systems, known as dactyloscopy, for criminals by law enforcement dating back to 1897 [3].

Human fingerprints are fully formed by the end of the first seven months of pregnancy on the unborn fetus and will remain constant throughout a lifetime. The exception to this is when a fingerprint is modified unintentionally from accidents like cuts and bruises. Fingerprints are so unique that the probability of any two being exactly alike is around one in 1.9×10^{15} [10], [11].

1.3.2 Function of an Automatic Identification System

An automatic identification system is one that determines a user's identity without having any prior information. This can be complicated because not having the user first claim to be a specific person requires the identification system to process the input image against all template images in the stored database. If the user has not previously had his/her template image loaded in the database, the system will fail at every attempt made to identify him/her [6].

The automatic identification system works by taking an input image from a user and performing a one-on-one comparison of the input image against each template image in the stored database. Then, it determines the class by selecting the template image that contains features which are most similar to those of the input image. An identification system is a "Who am I?" form of a recognition system [6].

1.4 Previous Work

This thesis furthers automatic fingerprint identification system research efforts in [12]. In his thesis, the author designs an automatic fingerprint identification system consisting of the following processing stages:

1. Image enhancement (or pre-processing),
2. Feature extraction and fusion,

3. Template image generation and
4. Correlation-based matching

The image enhancement stage consists of contrast stretching, local histogram equalization with image segmentation, local normalization, and image morphology. Then, in the feature extraction stage, the image is subjecting to binary thresholding followed by ridge direction and ridge density extracted locally as features via estimates from the two-dimensional Discrete Fourier Transform approach. After that, a new approach, known as “Pseudo Spectrum Fusion”, is taken to fuse the direction image and density image together resulting in a more unique feature. Next, the highest quality image from each class of fingerprint is chosen and a template image is generated and stored in a database. Finally, correlation-based matching is performed using an input test image against each of the template images from the stored database in a one-to-many fashion. The result is a fingerprint class for each match.

1.5 Objectives and Overview

Though the automatic fingerprint identification system developed in [12] was able to match up to 85% of the input images in a test database with their correct template image class, there is still room for improving the overall matching accuracy of the system. Exploring alternative matching schemes will be beneficial as well. The image enhancement algorithms should be improved to produce a result with more retained foreground (ridge) data for producing features, less noise and less unwanted background information. The direction image must be updated so that noise will be reduced when estimating ridge direction via the Discrete Fourier Transform approach. This promotes more accurate feature extraction estimates. In addition, alternative matching schemes will be tried with the goal of improving matching accuracy and reducing overall processing times.

This thesis is structured in the following manner. First, an overview of the baseline automatic fingerprint identification system developed in [12] is provided in Chapter 2. This reviews the image enhancement stage, feature extraction and fusion stage, and correlation-based matching stage. Areas for improvement in the baseline system are presented in Chapter 3. Following that, image enhancement modifications are covered in detail in Chapter 4, including contrast stretching and image segmentation. Next, is Chapter 5 that describes feature extraction modifications including quantization of the direction image. Then, Chapter 6 discusses alternative correlation-based matching schemes including single feature, two-channel features and multiple template images per class. Simulation experiment results follow in Chapter 7 where simulated matching runs are performed and the resulting matching test data is displayed in tables for the reader. This shows the matching accuracy improvements in a quantitative manner. The final section is Chapter 8, which describes conclusions drawn from this thesis and recommends future research.

CHAPTER 2

BASELINE AUTOMATIC FINGERPRINT IDENTIFICATION SYSTEM

The physical traits of the human fingerprint are discussed first in this chapter which is then followed by an overview of correlation-based identification systems. The last section provides a review of the baseline automatic fingerprint identification system designed in [12].

2.1 Analysis of a Fingerprint

The human fingerprint is used as a biometric identifier due to the unique characteristics of the ridges and valleys present on its surface. The ridges are denoted by black lines and the valleys are denoted by white lines shown in a binary (or black and white) fingerprint image. In 8-bit or 16-bit grayscale format, the darker-gray lines comprise the ridges and lighter-gray lines comprise the valleys [12].

The ridges on a fingerprint can be divided into two different categories of features, which can be analyzed and used for personal identification purposes. These two groups are called:

1. Minutiae structures and
2. Coarse level structures

Minutiae structures utilize the fine ridge details and include terminations/endings, bifurcations, loops, whorls and arches [5], [13]. These features are traditionally used in automatic fingerprint identification systems because they are considered more reliable. This is due to higher complexity in the matching system at the expensive of much longer processing times [3], [14], [15], [16]. The problems with using minutiae structures include heavy reliance on image quality and enhancement and error propagation between stages

in the system. Other sources of error include false minutiae and missing minutiae that are common when matching minutiae sets. Coarse level structures are analyzed on a larger scale and include the density (or frequency) of ridges per unit area and the direction (or orientation) in which the ridges flow within a certain region of area. Though less commonly used, these features are less sensitive to image quality with the added benefit of reduced processing time [17], [18]. Consequently, the coarse level features will be studied in this thesis.

2.2 Correlation-based Automatic Fingerprint Identification Systems

A correlation-based automatic fingerprint identification system (AFIS) functions by enhancing an input image, extracting and fusing feature data from that image and then performing cross-correlation matching with template images in a stored database. Cross-correlation matching is performed on the input fingerprint image and each of the template images in the stored database in a one-to-many fashion. The template image that produces the cross-correlation matrix with the largest, real-valued coefficient is selected as the match. The selected template image class is then assigned as the class of the input fingerprint image [12]. Figure 2.1 provides a block diagram of a correlation-based AFIS.

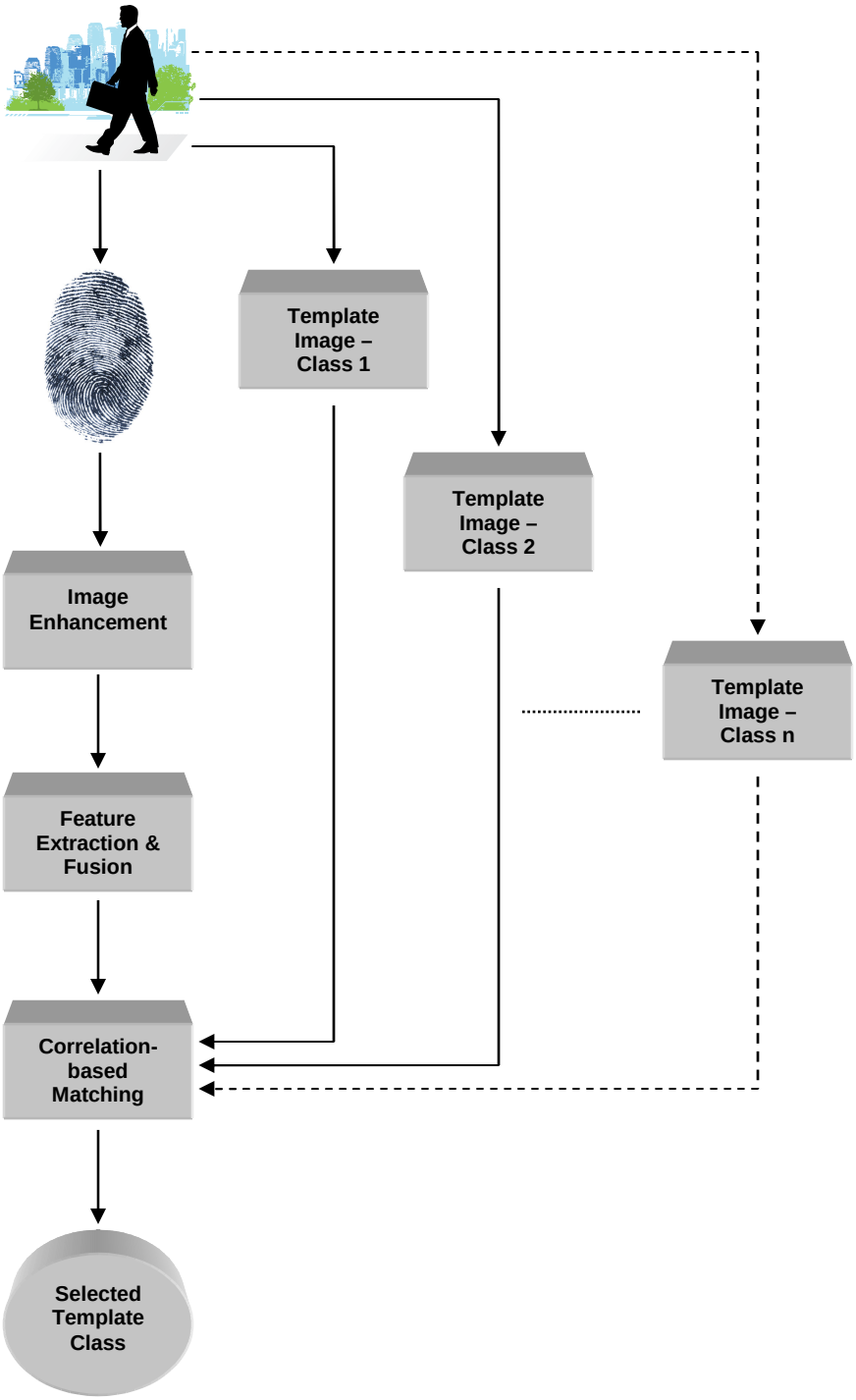

Figure 2.1 – Correlation-based Identification System Block Diagram

2.3 Review of the Baseline System

The following sub-sections review the baseline automatic fingerprint identification system developed in [12]. The review covers all stages of the system displayed in Figure 2.1 including image enhancement, feature extraction and fusion and correlation-based matching.

2.3.1 Image Enhancement Stage

The four types of image enhancement, including contrast stretching, local histogram equalization with image segmentation, local normalization and image morphology, are described under the proceeding sub-headings. The block diagram in Figure 2.2 displays the sequence in which the four image enhancement steps are performed.

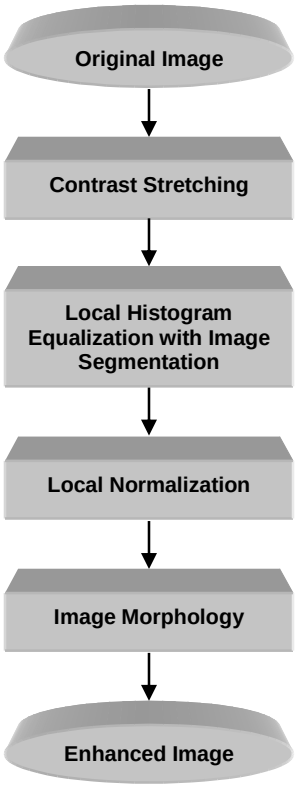

Figure 2.2 – Four Image Enhancement Steps Block Diagram

Before the four types of image enhancement are discussed, an explanation of how fingerprint image quality is determined is given.

2.3.1.1 Assessing Fingerprint Quality

Factors that affect image quality are the condition of the user's skin, the uniformity of physical contact made with the digital imaging device and the sensing capabilities of the digital imaging device. The condition can be altered via cuts and other physical damage to the skin. In addition, aging of the skin, along with an oily or dry surface, modifies the condition by changing the thickness of the ridges present. When physical contact with the digital imaging device is non-uniform, the fingerprint may be improperly captured. This non-uniform mapping often results in shift and rotational errors in the captured fingerprint image. Sensing capabilities of a digital imaging device that affect image quality include resolution and dynamic range. The resolution is represented by units of dots per inch (dpi) or pixels per inch (ppi). The dynamic range describes the number of intensity levels available for each pixel in the image and is measured in units of bits [12].

Visual evidence of low quality in a fingerprint image would be discontinuities in the ridges, smudges between them or thick background noise [12]. Examples of different quality fingerprint images are shown in Figure 2.3. The matching accuracy of an automatic fingerprint identification system is reduced when image quality is poor.

Figure 2.3 – Examples of Different Quality Fingerprint Images

Image enhancement techniques must be applied to the fingerprint images in order to allow for better feature extraction which increases the matching accuracy of the automatic identification system. Specifically, the following three ridge characteristics, when distorted, are targeted by the enhancement scheme:

1. Separation,
2. Discontinuity and
3. Background noise

If parallel ridges are not well separated due to noise, they may appear smudged or smeared together, which makes it more difficult to determine their orientation. If there are discontinuities in the ridges, this can be caused by uneven ridge intensity from poor lighting or damaged skin resulting in slight gaps or breaks. Background noise casts a shadow over the entire image which darkens it. This affects extraction of the features when ridges appear blurry and in some cases ridge structures are generated that did not previously exist. The three ridge characteristics mentioned above can drastically

degrade feature extraction in areas of the fingerprint image where they are corrupted [12].

2.3.1.2 Contrast Stretching

Low-contrast is exhibited in some areas of fingerprint images and can be observed as a small range of grayscale levels in a particular area. This is often caused by poor or non-uniform illumination, small dynamic range of the digital imaging device or nonlinearity of the digital imaging device [19].

The contrast stretching algorithm described in this subsection attempts to enhance the low-contrast areas of the image. This is accomplished by expanding the corresponding grayscale levels into a larger range. Contrast stretching is performed on both the region of interest known as "foreground" and the background region of the image. The algorithm described next demonstrates a simple contrast stretching transformation [12].

The following steps describe the contrast stretching algorithm used in the baseline automatic fingerprint identification system designed in [12]. Given $I(k,l)$ as the intensity image and the maximum grayscale level L, where the coordinates (k,l) denote the location of the grayscale pixel value in the range of 0 to $L-1$, the simple contrast stretching transformation is shown as:

$$C(k,l)=\begin{cases}\alpha\cdot I(k,l), & 0\le I(k,l)<a\\ \beta\cdot(I(k,l)-a)+V_a, & a\le I(k,l)<b\\ \gamma\cdot(I(k,l)-b)+V_b, & b\le I(k,l)<L\end{cases} \quad (2.1)$$

The most critical information in a fingerprint image is typically compressed into a small range of grayscale values. Careful selection of a and b in Equation 2.1 allows expansion of the ridge information into the maximum number of grayscale levels. The grayscale levels corresponding to values greater than b are denoted as background

information [12]. A side-by-side comparison of a fingerprint image before and after contrast stretching is shown in Figure 2.4. Notice that there is not much difference in the contrast using this simple transformation method.

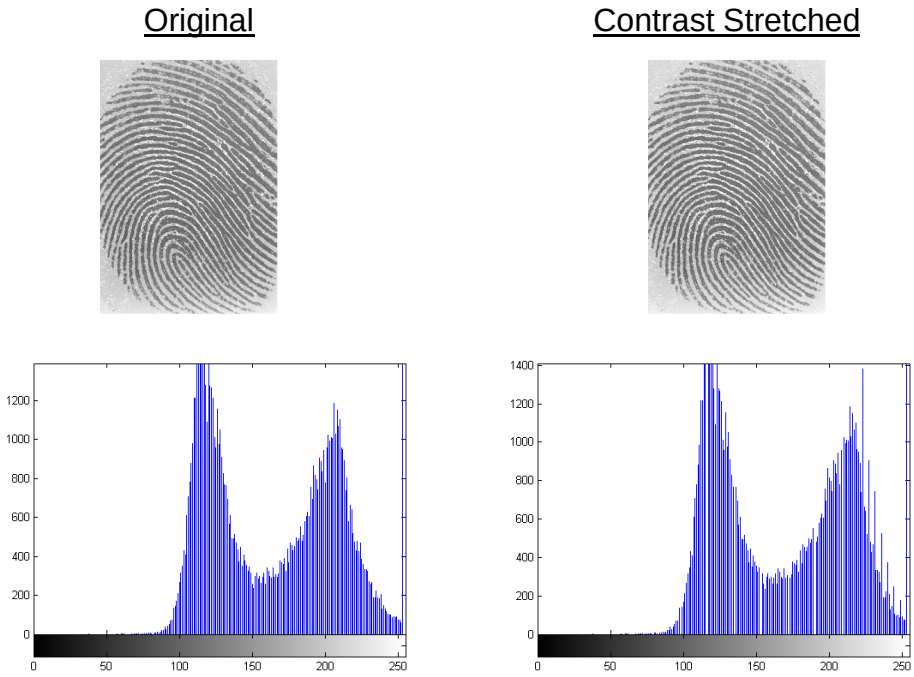

Figure 2.4 – Example of Contrast Stretching: Before and After (Baseline)

2.3.1.3 Local Histogram Equalization with Image Segmentation

After contrast stretching is completed, image segmentation, followed by local histogram equalization, is executed in order to eliminate background information and reduce inter-ridge smudges. Image segmentation separates the image into foreground (region of interest) areas for histogram equalization and background areas which are ignored. This not only facilitates faster, more efficient image processing at the current enhancement stage, but for future stages as well because image segmentation information is stored for later use. The local approach for histogram equalization enhances small areas of the image in the region of interest which brings out more fine

detail. This is a much better method than using a global approach which would enhance areas outside the region of interest and thus increase noise and add unnecessary processing time [12].

Before local histogram equalization can be performed, an image segmentation algorithm is run on the fingerprint image that designates which areas are foreground blocks and which are background blocks. A threshold value is generated for this purpose using the variance of a dxd pixel block within the image and works extremely well because background variance is much less than foreground variance. The exact threshold variance is calculated by first dividing the two-dimensional intensity array $I(k,l)$ into $M \cdot N$ blocks of size dxd pixels. Each block contains its own intensity array which is denoted as $I_{mn}(k,l)$. Then, a single threshold variance is computed with a scaling factor, α, in the following manner:

$$\sigma^2{}_{thresh} = \alpha \cdot \frac{1}{(d-1)^2} \sum_{l=0}^{d-1} \sum_{k=0}^{d-1} \left(I_{mn}(k,l) - \mu_{mn} \right)^2 \tag{2.2}$$

with the mean value of the block computed as:

$$\mu_{mn} = \frac{1}{d^2} \sum_{l=0}^{d-1} \sum_{k=0}^{d-1} I_{mn}(k,l) \tag{2.3}$$

This threshold variance is calculated from the block in the dead center of the fingerprint image [12]. The red block shown in Figure 2.5 below indicates the exact location of the pixel block used to compute the single threshold variance value.

Figure 2.5 – Single-Point Threshold Variance Location

Finally, each block in the two-dimensional intensity array $I(k,l)$ is subjected to the threshold variance. Those with a variance σ^2_{mn} that is greater than σ^2_{thresh} are denoted as foreground blocks and the remaining ones are denoted as background blocks [12].

Local histogram equalization is performed by transforming the grayscale values in each of the dxd pixel blocks with two-dimensional intensity array $I_{mn}(k,l)$ such that an equalized (or uniform) histogram is created. Define L as the number of grayscale values contained in the block. The initial block can be represented by its discrete histogram or discrete density function with the follow equation:

$$p_{\mathrm{l}mn}(l) = \frac{n_l}{d^2} \tag{2.4}$$

for l = 0, …, $L-1$, where n_l is the number of pixels in the block with grayscale level l. The process of histogram equalization maps the old grayscale values into new ones such that the new histogram is completely uniform. The transformed grayscale values, which must also be in the range of k = 0, …, $L-1$ can be represented by the transformed discrete histogram as follows [12]:

$$v_k = \sum_{l=0}^{k} p_{\mathrm{l}mn}(n_l) \tag{2.5}$$

Another side-by-side image and histogram comparison is shown in Figure 2.6 which gives a clear visual example of the results of performing local histogram equalization with image segmentation on a fingerprint image. A much more uniformly distributed histogram is evident from the local histogram equalization along with block-like patterns of enhancement throughout the resulting image from segmentation.

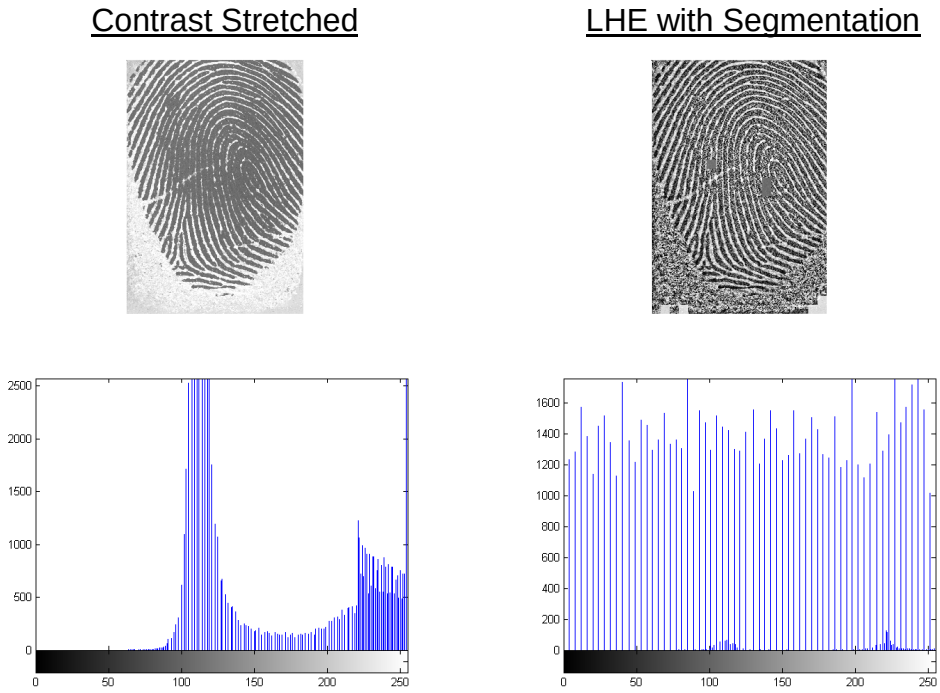

Figure 2.6 – Example of LHE with Image Segmentation: Before and After (Baseline)

2.3.1.4 Local Normalization

Local normalization is the next step of image enhancement and is applied to the fingerprint image in order to increase the contrast level between the ridges, which are dark gray to black in color, and valleys, which are light gray to white in color. This is necessary because the effects of the local histogram equalization that was applied previously enhanced both the ridges and the valleys. This resulted in valleys that appear

as darker shades of gray than desired. Sharpening of the contrast through local normalization will reverse these undesired effects on the valleys and thus provide a better result for feature extraction [12].

This algorithm is applied in a local fashion meaning that it will only affect the blocks that were designated as "foreground" during image segmentation in the previous subsection. It attempts to reduce the grayscale value differences along the ridges and valleys by setting the mean and variance of each local block to pre-determined values. Using pre-determined mean and variance values aids in sharpening the contrast which lowers the side-effects of the local histogram equalization on the valleys. For each dxd local pixel block with two-dimensional intensity array $I_{mn}(k,l)$, mean μ_{mn} and variance $\sigma_{mn}{}^2$, normalization is performed on each grayscale pixel using this formula:

$$\mathrm{N}_{mn}(k,l) = \begin{cases} \mu_0 + \sqrt{\dfrac{\sigma_0{}^2 \left(I_{mn}(k,l) - \mu_{mn}\right)^2}{\sigma_{mn}{}^2}} & I_{mn}(k,l) > \mu_{mn} \\ \mu_0 - \sqrt{\dfrac{\sigma_0{}^2 \left(I_{mn}(k,l) - \mu_{mn}\right)^2}{\sigma_{mn}{}^2}} & \textit{otherwise} \end{cases} \tag{2.6}$$

with pre-determined mean μ_0 and pre-determined variance $\sigma_0{}^2$ [12].

Figure 2.7 below shows the effects of local normalization on the individual pixels in the fingerprint image and it can be seen that the valleys have become brighter which produces more pronounced ridges.

LHE with Segmentation

Local Normalized

Figure 2.7 – Example of Local Normalization: Before and After (Baseline)

2.3.1.5 Image Morphology

The final step of image enhancement is image morphology which is performed with the goal of reducing and possibly removing pixel pits and holes. These blemishes are remnants of the local normalization that was done in the previous subsection. This operation is also known as "morphological opening" [12].

Image morphology is performed using the following procedure. First, the fingerprint image is zoomed in by a factor of two (2X) in order to allow room for the smoothing filter to be applied to the image without thickening the ridges or merging them together. Next, a smoothing filter, in the shape of a disk with a radius of one pixel, is applied to the entire image, which eliminates many of the pixel pits and holes. Given $I(k,l)$ as the two-dimensional intensity array of the fingerprint image, then Equation 2.7 describes the disk-shaped smoothing filter with a radius of one pixel:

$$M(k,l) = \min\{I(k+m, l+n)\} \qquad -1 \le m \le 1, \quad -1 \le n \le 1 \qquad (2.7)$$

Finally, the filtered image is zoomed out by a factor of one-half (0.5X) in order to return it to the original size [12].

Figure 2.8 provides a side-by-side display of a fingerprint image before and after the morphological opening process. Notice the reduction in random speckle noise throughout the image.

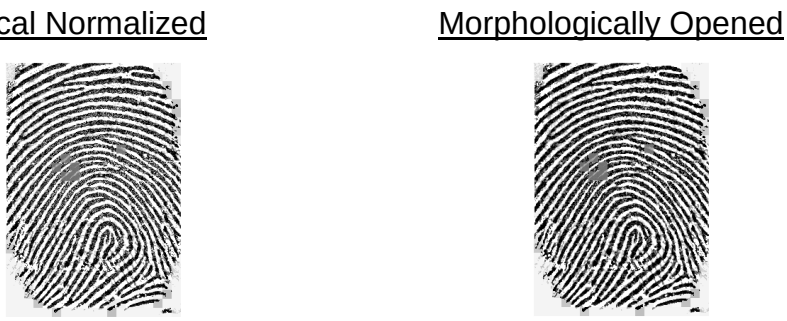

Figure 2.8 – Example of Morphological Opening: Before and After

2.3.1.6 Image Enhancement Results

Examples of actual fingerprints before and after image enhancement is applied are shown in Figure 2.9 below. The top row shown in the figure contains the original images and the bottom row contains the images after being exposed to all four steps of enhancement.

Figure 2.9 – Four Stages of Image Enhancement Examples (Baseline)

2.3.2 Feature Extraction and Fusion Stage

An extracted feature in an automatic fingerprint identification system provides a representation of the unique aspects of an individual. The feature must be implemented so that it performs optimally with the chosen matching scheme at a later stage in the system. This is necessary because the functionality of the two is interdependent. The feature extraction method has the largest influence on the type of design and level of performance of the automatic fingerprint identification system [12].

In order to qualify for use in an automatic fingerprint identification system, the extracted feature should meet certain criteria. This includes:

1. Rotation invariance (i.e. the image may be rotated at various angles on the digital imaging device while yielding the same extracted feature),
2. Shift invariance (i.e. the image may be shifted to another location on the digital imaging device while yielding the same extracted feature),

3. Noise immunity (i.e. the image will yield the same extracted feature even if different types of noise are present in itself or the digital imaging device) and
4. Memory storage efficiency (i.e. the amount of memory occupied by the extracted feature is much less than that of an 8-bit grayscale image; yet the amount of information contained is sufficient)

The chosen feature should satisfy most of the conditions mentioned above in addition to those conditions covered by the correlation-based matching stage [12].

The automatic fingerprint identification system covered in this thesis satisfies the requirements of slight rotation invariance, shift invariance, some noisy immunity and memory storage efficiency. Due to the preservation of fine details in a local-type feature, slight rotational invariance exists. Shift invariance is provided by the two-dimensional cross-correlation matching stage in the system. The four image enhancement steps provide a method for noise immunity. The final requirement, known as memory storage efficiency, is met through the use of block-wise operations for local features that significantly reduce the number of captured data points in comparison with pixel-wise operations. However, there is no negative impact on the extracted feature data [12].

2.3.2.1 Fingerprint Representation Overview

A fingerprint image contains unique features, or representations, that can be used for the purpose of identification. The features that are best qualified for fingerprint identification are those that remain unchanged in the presence of shift, rotation and other physical disturbances [20]. Representations can be classified as two different types:

1. Global features and
2. Local features

Global features, which include core and delta, are most often used to index and classify fingerprint images. They are comprised of a single feature covering the entire area that

provides a general, or overall, description of the fingerprint. This requires that the fingerprint be examined as one, large area. On the other hand, automatic identification system applications work well with local or minutiae features. This type consists of many features found on one fingerprint with each being captured from a different segment of the image [12].

The two local representations used in the baseline automatic fingerprint identification system in this thesis are ridge direction and ridge density. Ridge direction is a very popular type of local feature in the industry and indicates which way the ridges "flow" in a specific area of the image. It is also known as "ridge orientation" [21]. The second type of local representation, which isn't quite as popular, indicates the number of ridges contained in a particular area of the fingerprint image and is known as ridge density. Ridge density is often used for filter design, classification and identification purposes. It is also called "ridge frequency". Other local representation methods exist in the form of minutiae features which include terminations/endings, bifurcations, loops, whorls and other fine ridge details [12].

2.3.2.2 Ridge Direction Representation

There are two similar mathematical models that may be used to represent fingerprint ridge direction. The first is known as a "vector field" and is shown in the Cartesian plane in Figure 2.10 below.

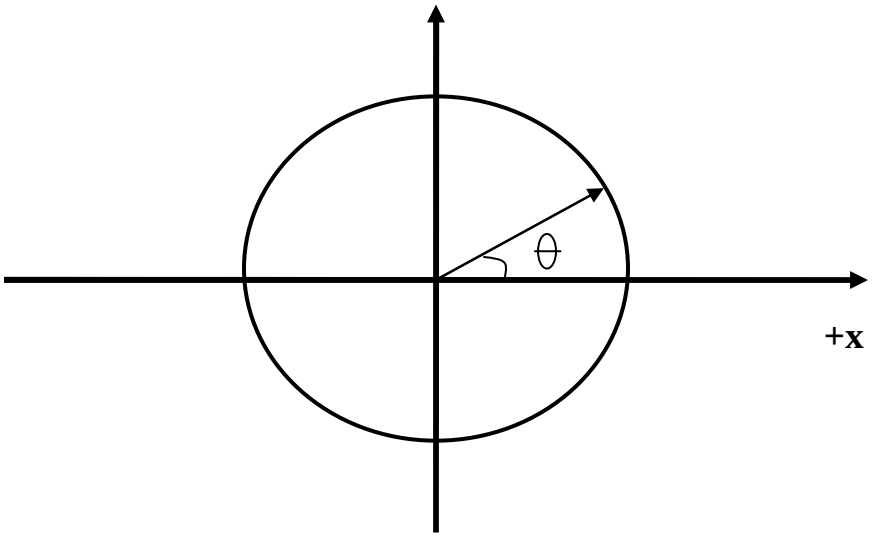

Figure 2.10 – Vector Field Model

The angle θ represents the direction of the vector and falls in the range of 0 to 2π radians with respect to the positive x-axis (or positive horizontal axis). The second mathematical model appears as a straight line in place of the vector and is known as an "orientation field" (or direction field). An example of it is displayed in another Cartesian plane in Figure 2.11 shown next.

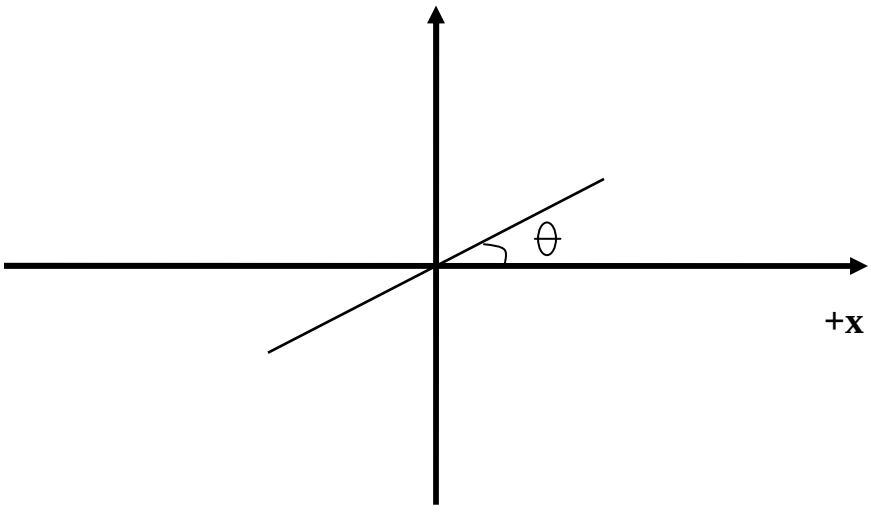

Figure 2.11 – Orientation Field Model

In this case, the angle θ now represents the orientation of a straight line. This angle θ is similar to the angle described in the vector field model because it is measured in radians with respect to the positive x-axis (or positive horizontal axis). However, its range is limited to 0 to π radians with no change in the angle θ when phase-shifted by integer multiples of π radians [12].

Both the vector field and orientation field are two-dimensional functions that model an angular direction. The vector field represents a direction in the range of 0 to 2π radians and the orientation field represents a direction in the range of 0 to π radians. The ridges of a fingerprint appear identical when phase-shifted by π radians (i.e. 0 and π, π/2 and 3π/2, π/4 and 5π/4) which makes the orientation field more suitable for modeling fingerprint ridge direction [12]. Hence, the orientation field is the one that will be used in this thesis.

2.3.2.3 Ridge Density Representation

The number of ridges present in a confined local area (or block) in the fingerprint image is known as ridge density (or "ridge frequency"). The unit of measurement consists of the width of one ridge and its neighboring valley combined. This is not to be confused with ridge distance which is measured as the length of a perpendicular line between two ridges beginning at the center of the first ridge and ending at the center of the second one [22]. Ridge density estimates can be affected by variables such as intra-fingerprint and inter-fingerprint ridge distances, ridge direction and different types of noise [12].

2.3.2.4 Direction and Density Images Overview

Direction and density images are the models that are used to store the extracted feature information which is later fused together. Generating the best possible estimates of both ridge direction and ridge density is especially critical since these two local representations describe an entire fingerprint image [12].

The direction image, $\theta(m,n)$, is comprised of a two-dimensional set of $M \cdot N$ blocks with each containing a local ridge direction. Each of these local ridge direction estimates is derived from the pixels in a dxd non-overlapping block in a fingerprint image. In addition to estimating ridge direction, the pixels in a dxd non-overlapping block in the fingerprint image are used to generate the ridge density estimate [12].

The density image, $D(m,n)$, is also comprised of a two-dimensional set of $M \cdot N$ blocks, but this time each contains a local ridge density estimate. This estimate is defined as the number of ridges along the direction perpendicular to the direction of the ridge orientation in a local area [12].

In the next two subsections, image thresholding and the two-dimensional Discrete Fourier Transform approach for estimating ridge direction and ridge density simultaneously are explain in detail [12].

2.3.2.5 Image Thresholding

Before the two-dimensional Discrete Fourier Transform approach can be applied to the fingerprint image for ridge direction and ridge density estimation, it must be converted into a binary (or black and white) format via image thresholding. This serves as a special type of image enhancement that aids the features estimation process by reducing harmonics in the frequency spectrum that can be attributed to grayscale level variations in the spatial domain [12].

The image thresholding technique used in the baseline automatic fingerprint identification system is known as the "peaks and valleys" method. First, the minimum and maximum grayscale levels are extracted from the $M \cdot N$ intensity image $I(k,l)$, respectively, as:

$$I_{\min} = \min\{I(k,l)\} \qquad 0 \le k \le M-1,\ 0 \le l \le N-1 \tag{2.8}$$

$$I_{\max} = \max\{I(k,l)\} \qquad 0 \le k \le M-1,\ 0 \le l \le N-1 \tag{2.9}$$

Using the information obtained from Equation 2.8 and Equation 2.9, the 256 grayscale bins in the 8-bit intensity image $I(k,l)$ are compressed into a smaller resolution in this fashion:

$$N_{Bins} = round\left\{\frac{I_{\max}}{(I_{\max} - I_{\min})/10}\right\} \tag{2.10}$$

Next, the grayscale pixel values in $I(k,l)$ are mapped into the new histogram via a transformation with N_{Bins} as the new number of equally spaced bins:

$$I_{comp}(k,l) = T\{I(k,l)\} \tag{2.11}$$

with the new bins centers defined by the following equation:

$$Centers(k) = \frac{255}{(N_{Bins}-1)} \cdot k \qquad 0 \le k \le N_{Bins}-1 \tag{2.12}$$

After that, the first and second peaks are located in the histogram of $I_{comp}(k,l)$ and the corresponding bin positions $Pos_{\max 1}$ and $Pos_{\max 2}$ are noted, respectively:

$$Counts(Pos_{\max 1}) = Counts_{\max 1} \tag{2.13}$$

$$Counts(Pos_{\max 2}) = Counts_{\max 2} \qquad Pos_{\max 1} \ne Pos_{\max 2}, \qquad Pos_{\max 1} - Pos_{\max 2} \ne 1 \tag{2.14}$$

Finally, a threshold mean, μ_{thresh}, is computed from the values obtained in Equation 2.13 and Equation 2.14 using this formula:

$$\mu_{thresh} = \frac{Centers(Pos_{\max 1}) + Centers(Pos_{\max 2})}{2} \tag{2.15}$$

Taking the value obtained for the threshold mean, μ_{thresh}, the image thresholding operation is performed on the $M \cdot N$ intensity image $I(k,l)$ [12]:

$$I_{thresh}(k,l) = \begin{cases} 255 \ (white) & I(k,l) > \mu_{thresh} \\ 0 \quad (black) & otherwise \end{cases} \tag{2.16}$$

The side-by-side fingerprint image comparison shown in Figure 2.12 demonstrates the effects of image thresholding. It can be seen that the image is no longer in an 8-bit grayscale format, but has been converted into two-color binary instead.

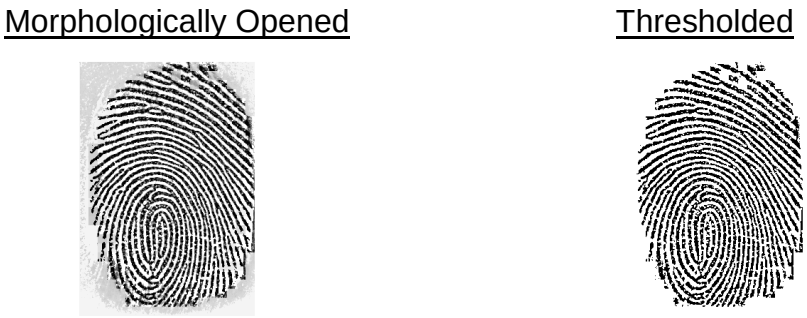

Figure 2.12 – Example of Image Thresholding: Before and After (Baseline)

2.3.2.6 Features Estimation Using Discrete Fourier Transform Approach

The Discrete Fourier Transform approach is used to estimate the local ridge direction and local ridge density for each fingerprint image. This approach locates a peak in the two-dimensional frequency magnitude spectrum from which to derive the ridge direction and ridge density estimates. The peak is a result of sinusoidal variations in brightness shown in the grayscale pixels in the spatial domain. This method is

advantageous over other available methods because it performs simultaneous computation of the local ridge direction and local ridge density, which allows much faster processing. Orientation and spacing of the ridges do not affect the results in the frequency magnitude spectrum resulting in more accurate estimates of direction and density [23].

The two-dimensional Discrete Fourier Transform approach is performed in the following manner. First, the fingerprint image is divided into $M \cdot N$ local blocks where each contains at least two ridge-valley pairs. This ensures a more accurate estimate of local ridge direction and local ridge density. Then, the two-dimensional Discrete Fourier Transform is performed on each block of size dxd with two-dimensional intensity array $I_{mn}(s,t)$ using the following formula:

$$U_{mn}(k,l) = \sum_{t=0}^{d-1}\sum_{s=0}^{d-1} I_{mn}(s,t) W_d^{(ks+lt)} \qquad 0 \le s,t,k,l \le d-1 \tag{2.17}$$

where W_d is given by the equation:

$$W_d = \exp\left(\frac{-j2\pi}{d}\right) \tag{2.18}$$

In order to simplify the estimation, only half of the frequency magnitude spectrum coefficients are used. This is permitted due to the symmetry property of the two-dimensional Discrete Fourier Transform [24]. In the next step, the coefficients are re-ordered as:

$$A_{mn}(f_x, f_y) = \left|U_{mn}(k,l)\right| \tag{2.19}$$

with f_x and f_y denoted as normalized frequencies in the ranges of:

$$0 \le f_x \le \frac{1}{2}, \quad -\frac{1}{2} \le f_y \le \frac{1}{2} \tag{2.20}$$

Before searching for a peak in the frequency magnitude spectrum, the DC component must be set to zero. It will always have the largest value, but contains no useful information for estimating local ridge direction and local ridge density. With the DC component set to zero, a search is performed on the spectrum to locate the next largest peak. The horizontal and vertical distances of this peak from the center of the frequency magnitude spectrum are used to estimate the ridge direction and ridge density. Specifically, the ridge direction estimate is obtained from the angle and the ridge density estimate is obtained from the length of the hypotenuse of the right triangle formed from the horizontal and vertical distance vectors [12].

Examples of the effect that different ridge-valley patterns have on the frequency magnitude spectrum can be shown using alternating black and white lines at various orientations. Figure 2.13 below displays the black and white patterns on the top row with the corresponding re-ordered frequency magnitude spectrums shown on the bottom row.

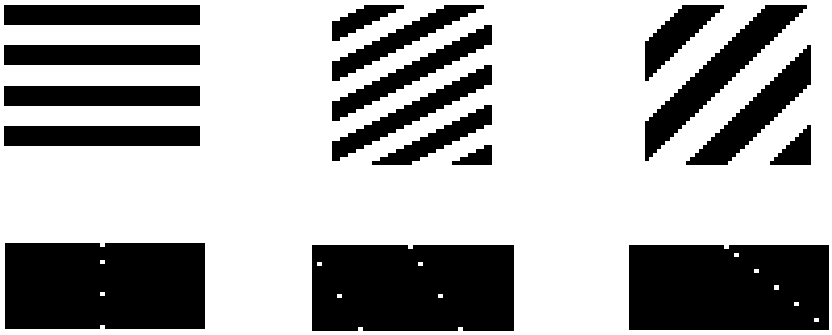

Figure 2.13 – Sample Patterns with Corresponding Re-Ordered Frequency Spectrums

The DC component is denoted on the three frequency magnitude spectrums in Figure 2.13 by the white pixel shown in the top-center. The white pixel located closest to the DC component is the peak of interest from which the ridge direction and ridge density estimates are derived [12].

Using the normalized frequency coordinates (f_x , f_y) obtained from the peak in the re-ordered frequency magnitude spectrum, the ridge direction is estimated using the following equation:

$$\theta = \arctan\left(\frac{f_y}{f_x}\right) \tag{2.21}$$

and the ridge density is estimated using this equation [12]:

$$D = \sqrt{f_x{}^2 + f_y{}^2} \tag{2.22}$$

Besides producing ridge direction and density estimates at faster speeds due to simultaneous computation, the Discrete Fourier Transform approach also provides a higher degree of accuracy than other methods. This is because the values calculated for the ridge direction estimates are not quantized to specific angles. To further enhance the accuracy of this approach, filtering or two-dimensional interpolation can be performed around the area of the peak [12].

Examples of ridge patterns taken from actual fingerprints along with their corresponding re-ordered frequency magnitude spectrums are displayed in Figure 2.14. The ridge patterns are along the left-hand column and the frequency spectrums are in the right-hand column. Notice the black pixel in the top-center of each frequency spectrum that represents the DC component after its value has been set to zero [12]. The frequency magnitude spectrums are zoomed in to allow the reader to clearly locate the peak in each.

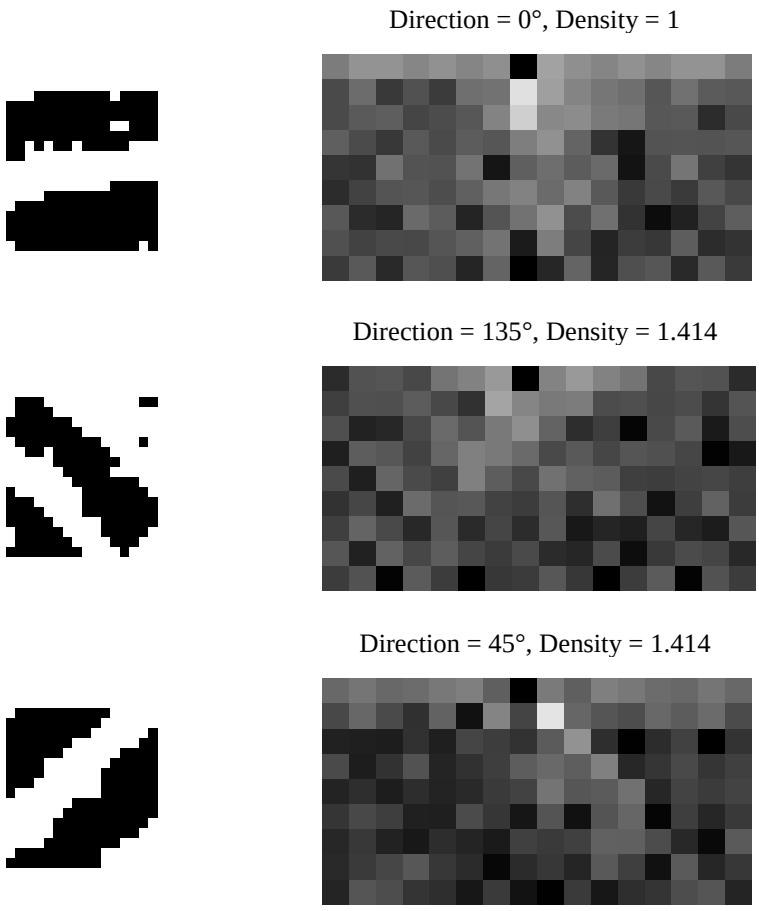

Figure 2.14 – Actual Fingerprint Ridge Patterns with Re-Ordered Frequency Spectrums

2.3.2.7 Direction and Density Images Results

Figure 2.15 provides two examples of actual fingerprints with their associated direction image and density image. The direction images and density images were obtained using the Discrete Fourier Transform approach discussed in the previous subsection.

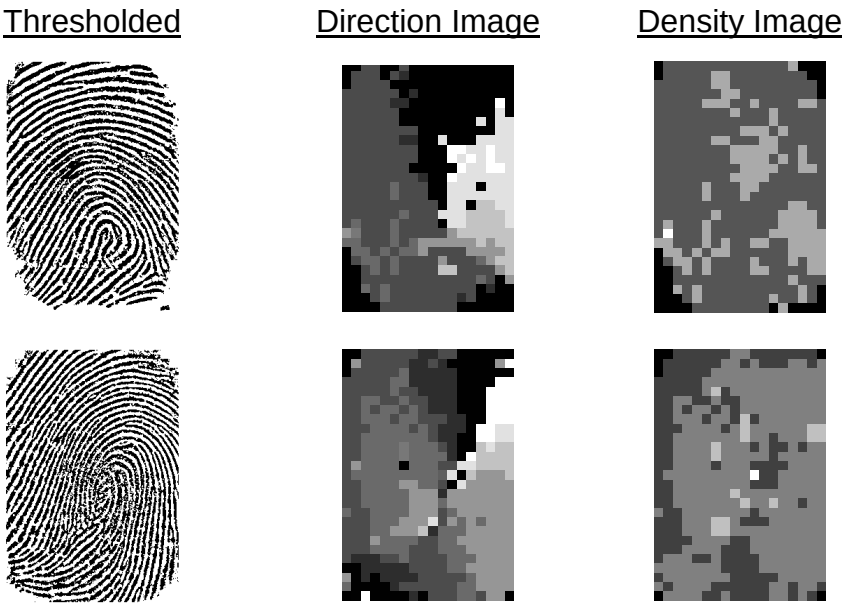

Figure 2.15 – Direction Image and Density Image Examples (Baseline)

2.3.2.8 Pseudo Spectrum Fusion

The two-dimensional Discrete Fourier Transform shown in Equation 2.17 provides the basis for the concept of pseudo spectrum fusion. The name "pseudo spectrum" stems from using frequency spectrum components (i.e. phase and magnitude) to represent spatial domain features (i.e. ridge direction and ridge density). This process combines the information contained separately in the direction image and density image into a single, fused feature. As an example, a digital image can be transformed and represented in the frequency domain as $U(k,l)$. This transformed image is complex and can be expressed in polar form as shown here:

$$U(k,l) = \left|U(k,l)\right| \cdot \exp(j\phi(k,l)) \tag{2.23}$$

where $\left|U(k,l)\right|$ stands for the magnitude and $\phi(k,l)$ represents the phase angle of the frequency spectrum [12].

Given the ridge direction θ and ridge density D, this same approach can be applied to create the fused feature F. The direction acts as the phase angle component and the density behaves as the magnitude component in the Discrete Fourier Transform. The extracted pseudo spectrum feature F, which is complex in nature, is described by the following equation:

$$F(m,n) = D(m,n) \cdot \exp(j2 \cdot \theta(m,n)) \quad (2.24)$$

Make sure to note that there is a factor of two multiplied by the ridge direction in Equation 2.24 with the purpose of eliminating discontinuities in the frequency spectrum. This also expands the range of angles from 0 - π to 0 - 2π. Figure 2.15 provides an example of this type of discontinuity [12].

The next subsection describes the correlation-based matching scheme used in the baseline automatic fingerprint identification system.

2.3.3 Correlation-based Matching Stage

The purpose of a matching scheme is to compare the unique traits of an input image with a template image and then report the degree of similarity or a decision on whether or not they are from the same class. Most matching schemes do not directly compare grayscale pixel values, but instead use features that are extracted prior to the matching stage. The form of recognition chosen often dictates the type of extracted feature used by the matching scheme. As an example, an identification system requires local features such as ridge direction and ridge density, but a classification system uses global features including cores and deltas [12].

The variation in appearance of fingerprint images makes the task of devising a matching scheme with a high degree of accuracy very challenging. Most of the requirements that qualify a local feature for identification system purposes are satisfied prior to the matching stage. These include rotation invariance, noise immunity and

memory storage efficiency. This leaves the matching stage to compensate for the shift invariance property [12].

The matching scheme chosen for the baseline automatic fingerprint identification system uses a "correlation-based" technique. The process involves taking an input grayscale image and template grayscale image (or input feature image and template feature image) and superimposing them on top of one another. Then, two-dimensional cross-correlation is performed on corresponding pixels in the case of the former (or corresponding features in the case of the latter). In either case, the cross-correlation is executed at various alignments of the two images before the process is completed. The different alignments of the images during cross-correlation invoke the shift invariance property mentioned earlier in this chapter. For example, an input image $I(k,l)$ and selected template image T_p produce the cross-correlation matrix $C_{IT}(m,n)$ based on all points in the input image, where p denotes the p th template. This is represented by the following equation [12]:

$$C_{IT}(m,n) = \sum_{l=0}^{N-1}\sum_{k=0}^{M-1} I(k,l){T_p}^{*}(k+m,l+n) \qquad -M \le m \le M,\ -N \le n \le N \quad (2.25)$$

The correlation-based matching scheme described above would not be practical when used for direct grayscale image comparison due to the extremely large number of computations required for pixel-wise operations. However, since the identification system uses local features instead of grayscale pixels, there are far fewer data points to process during cross-correlation. Thus, the formula in Equation 2.25 shown above is satisfactory [12].

Another possible matching scheme uses a "minutiae-based" technique and is more common in automatic fingerprint identification systems currently available. Minutiae

matching schemes extract features from an input image and a template image and store them as locations and orientations in a two-dimensional plane. Then, the planes are aligned such that a maximum number of minutiae pairings are achieved. An advantage to using the "minutiae-based" approach is that it can compensate for images with a very high degree of rotation, but is computationally expensive resulting in much longer match processing times [12].

2.3.3.1 Fused Features Matching

The matching scheme in the baseline automatic fingerprint identification system is correlation-based and operates on extracted features generated by the Pseudo Spectrum Fusion approach. The fused features matching process is performed with the following steps:

1. A high-quality fingerprint image from each class in a given database is chosen to become a template image. Each of these selected images is enhanced followed by feature extraction and fusion. The fused features from each selected fingerprint image are saved into a template image and stored in a template database. Each is denoted as F_{Tp}, where p represents the template class.
2. Next, an input fingerprint image is selected from the same given database. It is enhanced followed by feature extraction and fusion. The fused features from the input fingerprint image are saved into an input features image and denoted as F_{In}, where n represents the input fingerprint class.
3. Cross-correlation is then performed on the first template image and input features image using Equation 2.25. The resulting cross-correlation matrix contains complex coefficients due to the complex nature of the fused features in F_{Tp} and F_{In}. Only the real part of the cross-correlation coefficients matrix is considered when determining

the degree of similarity between the template image and input features image. Large, real-valued correlation coefficients indicate a high degree of similarity between the two feature images where as small, real-valued correlation coefficients imply the two images are not at all alike.

4. The same input features image is then cross-correlated with each of the remaining template images stored in the template database. A match is determined by comparing the real-valued coefficients from each cross-correlation matrix with the rest and choosing the one with the largest, real-valued coefficient. For example, if the largest, real-valued cross-correlation coefficient results from crossing the input features image with template p, then the input features image is considered to match with finger p. A correct match results when p is equal to n.
5. The process described in Step 2 – Step 4 is then repeated for all input features images obtained from the given database. This assigns a template image class to every input features image [12].

It is easily observed that when a template image is determined a non-match with a given input features image, the resulting cross-correlation matrix contains small real-valued coefficients. Another indicator of a non-match is a cross-correlation matrix with coefficients that are large, negative real values. Both cases support the decision of a non-match since small or large, negative real-valued cross-correlation coefficients indicate a low degree of similarity [12].

2.3.3.2 Correlation-based Matching Results

The following examples in Figure 2.16, Figure 2.17 and Figure 2.18 provide a visual demonstration of the “correlation-based” matching scheme used in the baseline automatic fingerprint identification system. Three correlation-based matching scenarios are presented and they include:

1. Two identical images,
2. Two different images from the same fingerprint class and
3. Two different images from different fingerprint classes

In each example, the real-valued cross-correlation coefficients matrices are shown in three-dimensional mesh grid plots for the direct grayscale and Pseudo Spectrum Fusion approaches. Take note that since the direct grayscale approach is a pixel-wise operation and the Pseudo Spectrum Fusion approach is a block-wise operation, the sampling rates differ. The two fingerprint images used as the template image and input features image in the examples are shown above the three-dimensional mesh grid plots for reference [12].

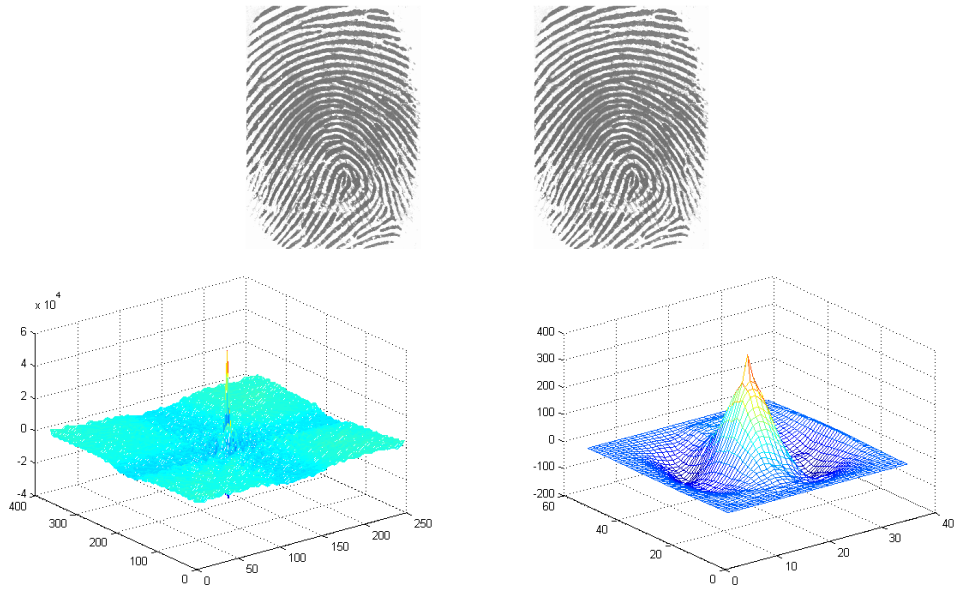

Direct Grayscale Approach

Pseudo-Spectrum Fusion Approach

Figure 2.16 – Correlation-based Matching: Exact Same Images

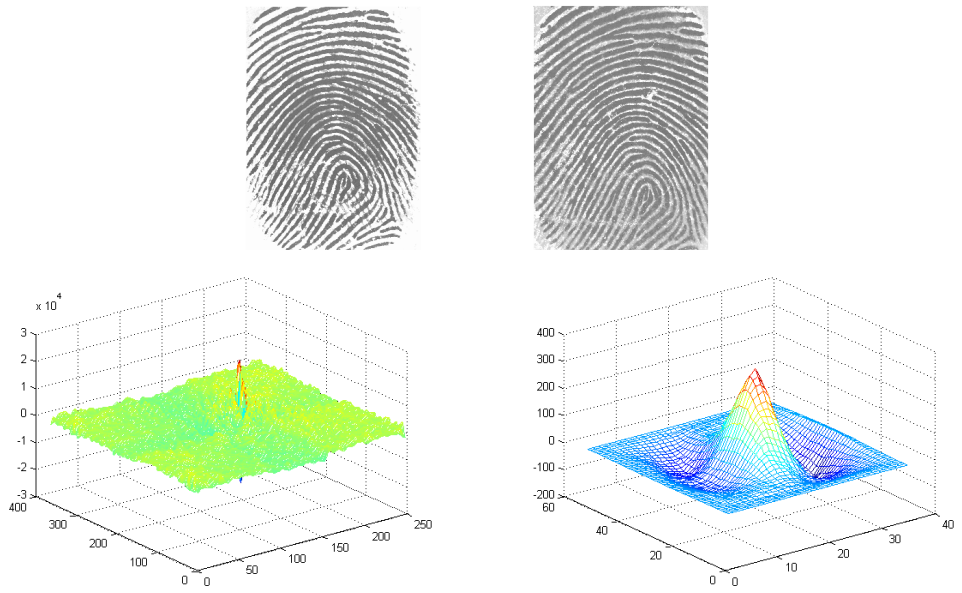

Direct Grayscale Approach

Pseudo-Spectrum Fusion Approach

Figure 2.17 – Correlation-based Matching: Different Images from Same Class

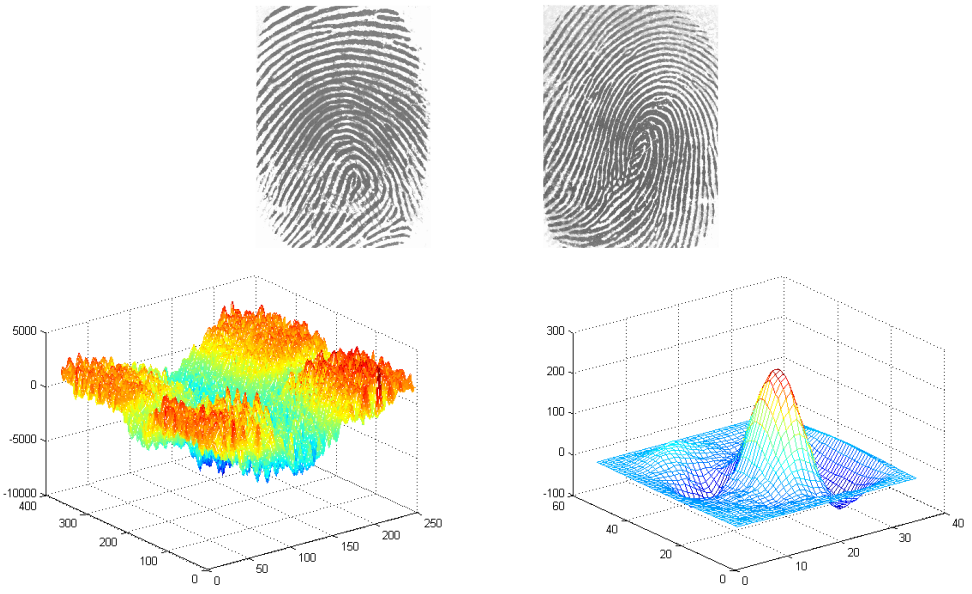

Direct Grayscale Approach

Pseudo-Spectrum Fusion Approach

Figure 2.18 – Correlation-based Matching: Different Images from Different Classes

The examples shown in Figure 2.16, Figure 2.17 and Figure 2.18 verify the correlation-based matching scheme works. When the two fingerprint images are a correct match, as in Figure 2.16 and Figure 2.17, large, real-valued cross-correlation coefficients are associated with the three-dimensional mesh grid plots. The visual indicator for this is the large peak in any one of the plots shown in Figure 2.16 or Figure 2.17. For the two fingerprint images that belong to separate classes in Figure 2.18, the real-valued cross-correlation coefficients are smaller which indicates a non-match. The visual indicator for this is a much smaller peak in either of the three-dimensional mesh grid plots shown in Figure 2.18 [12].

2.3.4 Overall Performance Results

In order to benchmark improvements, the overall matching performance results from the baseline automatic fingerprint identification system are summarized in Table 2.1 below. Details concerning the fingerprint database description, experiment setup and experiment observations are discussed later in Chapter 7.

Table 2.1 – Overall Matching Performance Results (Baseline)

	Fingerprint DB #1	**Fingerprint DB #2**	**Fingerprint DB #3**
Direct Grayscale	68.75%	83.75%	71.25%
Pseudo-Spectrum Fusion	70%	85%	82.5%

CHAPTER 3

AREAS FOR IMPROVEMENT

This chapter covers areas eligible for improvement in the baseline automatic fingerprint identification system and also provides a summary of the implemented solutions which are intended to increase the overall matching accuracy. Its purpose is to transition the reader from the review of the baseline system into the proceeding chapters in this thesis where components in the system are either modified or replaced along with quantitative evaluations that support these changes.

3.1 Problems to be Addressed

After careful review and evaluation of the baseline automatic fingerprint identification system in [12], the following components were selected for modification or replacement:

1. Contrast Stretching (image enhancement stage),
2. Image segmentation (image enhancement stage),
3. Direction Image (feature extraction and fusion stage) and
4. Fused features matching (correlation-based matching stage)

The contrast stretching algorithm discussed in Section 2.3.1.2 and demonstrated in Figure 2.4 results in little or no improvement in the contrast of the fingerprint image or the pixel distribution in the associated histogram. A new algorithm, which spreads out the pixels into a wider dynamic range, without changing the histogram shape, is desired. This will ensure much greater contrast between the ridges and valleys in the fingerprint image.

The image segmentation algorithm covered in Section 2.3.1.3 and demonstrated in Figure 2.6 results in loss of critical foreground information and retention of unnecessary background information, which lowers matching accuracy, slows down processing time and imposes unwanted noise in the system. A new algorithm, which generates a more accurate threshold for segmenting the image into foreground and background blocks, is desired. This will produce an image with the maximum foreground information and much less unwanted background information.

The ridge direction representation discussed in Section 2.3.2.2 – Section 2.3.2.4 and demonstrated in Figure 2.11 results in a direction image that retains much of the noise present in the fingerprint image. A new ridge direction representation, which reduces noise while retaining the maximum amount of direction feature data, is desired. This will produce a direction image that contains the most accurate ridge direction estimates generated during feature extraction.

The fused features matching algorithm discussed in Section 2.3.3.1 and demonstrated in Figure 2.16, Figure 2.17 and Figure 2.18 results in many correct matches, but certainly leaves room for exploring alternative matching schemes. New approaches to correlation-based matching, which utilize the same extracted features as the old matching scheme, are desired. Experimentation with alternative matching schemes may improve overall matching accuracy as well as pave the way for future research.

3.2 Thesis Goal and Tasks

The next three chapters contain details for the modifications performed on the image enhancement stage, feature extraction and fusion stage and correlation-based matching stage with a goal of improving the baseline system. First, Chapter 4 covers improvements in the image enhancement stage. This includes:

1. Replacing the simple contrast stretching transformation with a new algorithm referred to as the “contract and stretch” method and
2. Modifying the image segmentation algorithm to use a threshold variance to mean ratio computation for segmenting into foreground and background blocks

Next, improvements in the feature extraction and fusion stage are explained in Chapter 5. This includes quantizing ridge direction estimates in the direction image into four discrete levels. Finally, Chapter 6 covers experiments in the correlation-based matching stage. The alternative matching schemes explored include:

1. Direction only features matching,
2. Density only features matching,
3. Two channels with addition-type fusion matching,
4. Two channels with multiplication-type fusion matching and
5. Two templates per class matching

Each of the three proceeding chapters contains detailed descriptions of the new algorithms along with performance evaluations.

CHAPTER 4

IMAGE ENHANCEMENT IMPROVEMENTS

Details for the replacements or modifications performed on the image enhancement stage of the baseline automatic fingerprint identification system are discussed in this chapter. Each new algorithm description is followed by a performance evaluation for justification.

4.1 Contrast Stretching

The following contrast stretching algorithm is called the "contract and stretch" method which replaces the simple transformation found in the baseline system.

4.1.1 Algorithm Description

The "contract and stretch" method for contrast stretching is described in [25] and is provided in the following steps. Let $I(k,l)$ be the $M \cdot N$ two-dimensional intensity array of an 8-bit grayscale fingerprint image. First, the mean grayscale value of the entire image (or global mean) is computed by this equation:

$$\mu_0 = \frac{1}{M \cdot N} \sum_{l=0}^{N-1} \sum_{k=0}^{M-1} I(k,l) \tag{4.1}$$

Using μ_0 computed in Equation 4.1, the foreground peak, μ_{FG}, and background peak, μ_{BG}, can be located with the following:

$$\mu_{FG} = \frac{1}{N_{FG}} \sum_{i=1}^{N_{FG}} I(k,l) \qquad I(k,l) \le \mu_0 \tag{4.2}$$

$$\mu_{BG} = \frac{1}{N_{BG}} \sum_{i=1}^{N_{BG}} I(k,l) \qquad I(k,l) > \mu_0 \tag{4.3}$$

Note that N_{FG} indicates the number of grayscale pixels with values less than or equal to μ_0 (foreground pixels) and N_{BG} indicates the number of grayscale pixels with values greater than μ_0 (background pixels). Next, the standard deviations about the foreground peak, μ_{FG}, and background peak, μ_{BG}, are computed using these formulas:

$$\sigma_{FG} = \sqrt{\frac{1}{N_{FG}} \sum_{i=1}^{N_{FG}} \left(I(k,l) - \mu_{FG}\right)^2} \qquad I(k,l) \le \mu_0 \tag{4.4}$$

$$\sigma_{BG} = \sqrt{\frac{1}{N_{BG}} \sum_{i=1}^{N_{BG}} \left(I(k,l) - \mu_{BG}\right)^2} \qquad I(k,l) > \mu_0 \tag{4.5}$$

Then, the grayscale pixels are contracted to fit within the limits of $\mu_{FG} - \sigma_{FG}$ and $\mu_{BG} + \sigma_{BG}$:

$$I_{contract}(k,l) = \begin{cases} \mu_{FG} - \sigma_{FG} & I(k,l) < \mu_{FG} - \sigma_{FG} \\ \mu_{BG} + \sigma_{BG} & I(k,l) > \mu_{BG} + \sigma_{BG} \\ I(k,l) & otherwise \end{cases} \tag{4.6}$$

In the final step, the grayscale pixels are stretched into all 255 levels contained in the 8-bit grayscale range with the following equation:

$$I_{stretch}(k,l) = 255 \cdot \frac{I_{contract}(k,l) - (\mu_{FG} - \sigma_{FG})}{(\mu_{BG} + \sigma_{BG}) - (\mu_{FG} - \sigma_{FG})} \tag{4.7}$$

The side-by-side comparison of fingerprint images and associated histograms shown in Figure 4.1 provides a visual demonstration of the “contract and stretch” method for contrast stretching.

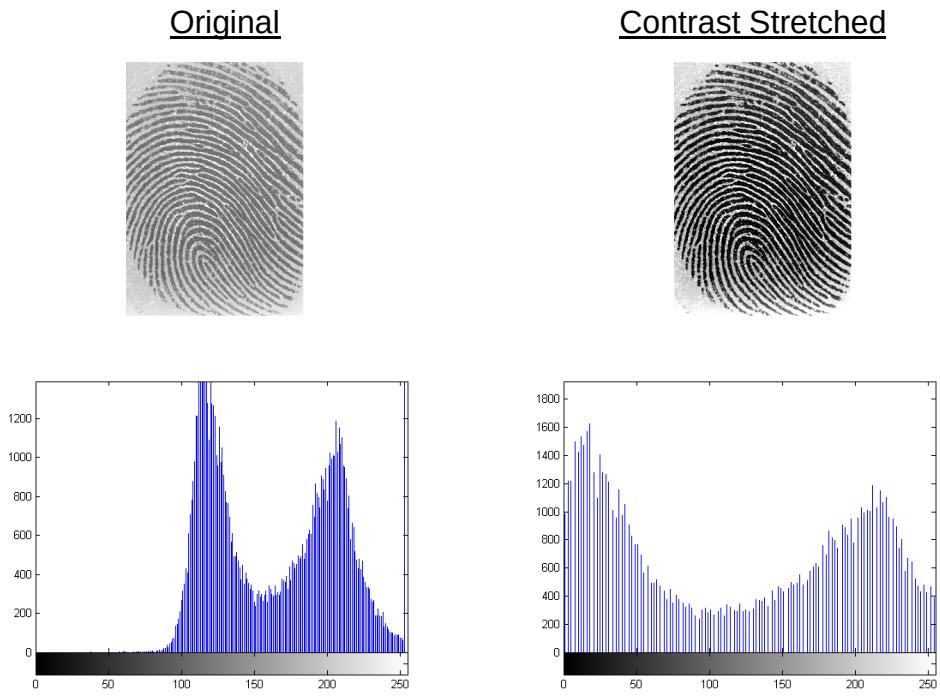

Figure 4.1 – Example of Contrast Stretching: Before and After (Improved)

4.1.2 Performance Evaluation

The enhanced fingerprint image and its associated grayscale histogram shown in Figure 4.1 demonstrate satisfaction of the requirement for a contrast stretching algorithm that expands the grayscale pixels into a much wider dynamic range without altering the shape of the pixel distribution in the histogram. As visual evidence in favor of the new algorithm, the enhanced image on the right hand side exhibits greater contrast between the ridges and valleys. Its grayscale histogram contains a pixel distribution which spans all 256 levels in the 8-bit range and retains the general shape of the distribution shown in the original grayscale histogram.

A matching accuracy test is also used to evaluate the performance of the new contrast stretching algorithm. The “contract and stretch” method was implemented in the

baseline automatic fingerprint identification system, which replaces the simple transformation, and simulated test runs were performed. The overall matching accuracy results have improved for DB #1 and DB #3, but remained unchanged for DB #2. They are shown in Table 4.1 below.

Table 4.1 – Matching Results (Contrast Stretching Improved)

	Fingerprint DB #1	**Fingerprint DB #2**	**Fingerprint DB #3**
Pseudo-Spectrum Fusion	81.25%	85%	87.5%

4.2 Image Segmentation

The following image segmentation algorithm uses a threshold variance to mean ratio for segmenting into foreground and background blocks which is a modified version of the threshold variance method used in the baseline system. The idea behind this new method for image segmentation is to take into account the grayscale mean as well as the variance in order to produce a more accurate threshold for segmenting blocks into foreground and background.

4.2.1 Algorithm Description

The proceeding steps describe the modified image segmentation algorithm that is run on the fingerprint image after contrast stretching is completed. A threshold value must be generated first using the global variance and global mean of the fingerprint image. The global variance, $\sigma^2{}_0$, is calculated from the $M \cdot N$ two-dimensional intensity array $I(k,l)$ using the following equation:

$$\sigma^2{}_0 = \frac{1}{(M-1)(N-1)} \sum_{l=0}^{N-1} \sum_{k=0}^{M-1} \left(I(k,l) - \mu_0 \right)^2 \tag{4.8}$$

with the global mean, μ_0, computed as:

$$\mu_0 = \frac{1}{M \cdot N} \sum_{l=0}^{N-1} \sum_{k=0}^{M-1} I(k,l) \tag{4.9}$$

Next, the threshold variance to mean ratio, $\frac{\sigma^2}{\mu}_{thresh}$, is chosen using the following calculation with a scaling factor, α :

$$\frac{\sigma^2}{\mu}_{thresh} = \alpha \cdot \frac{\sigma^2{}_0}{\mu_0} \tag{4.10}$$

Finally, the two-dimensional intensity array $I(k,l)$ is divided into dxd pixel blocks and each is subjected to the threshold variance to mean ratio. Those with a local variance to local mean ratio that is greater than $\frac{\sigma^2}{\mu}_{thresh}$ are denoted as foreground blocks and the remaining ones are denoted as background blocks [26].

Following image segmentation, local histogram equalization is performed by transforming the grayscale values in each of the dxd pixel blocks with two-dimensional intensity array $I_{mn}(k,l)$ such that an equalized (or uniform) histogram is created. A detailed procedure describing the steps for local histogram equalization is provided in Section 2.3.1.3 of Chapter 2.

Another side-by-side comparison of fingerprint images and associated histograms is shown in Figure 4.2 and provides a visual demonstration of the threshold variance to mean ratio method for image segmentation.

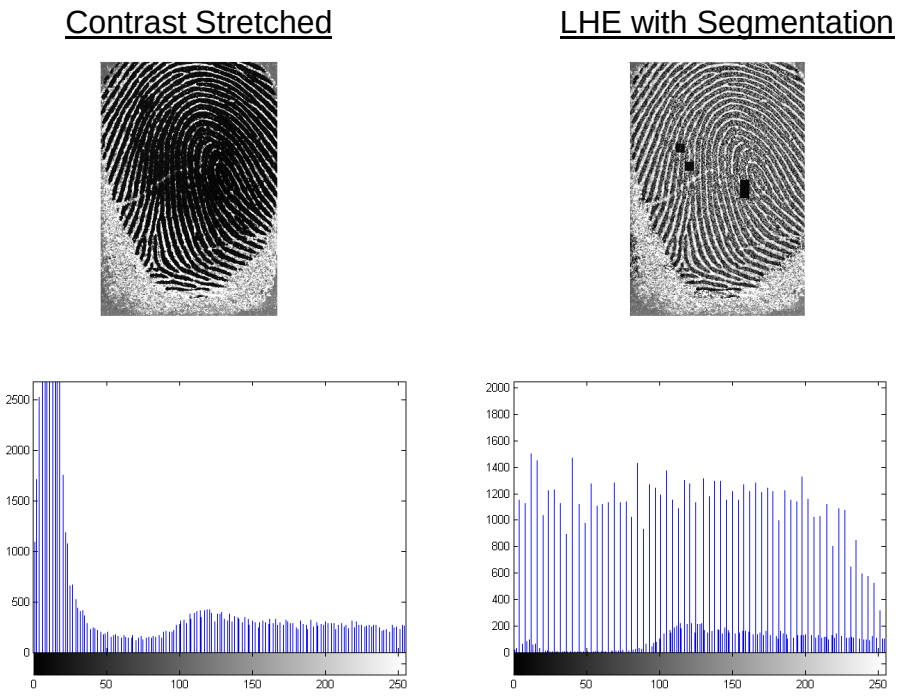

Figure 4.2 – Example of LHE with Image Segmentation: Before and After (Improved)

4.2.2 Performance Evaluation

The enhanced fingerprint image and its associated grayscale histogram shown in Figure 4.2 demonstrate satisfaction of the requirement for an image segmentation algorithm that retains the maximum critical foreground information with less unnecessary background information in order to increase matching accuracy, reduce noise and increase processing speed. As visual evidence in favor of the new algorithm, the enhanced image on the right hand side exhibits more foreground information and less background information. Its grayscale histogram appears equalized (or uniform) indicating local histogram equalization has been performed.

A matching accuracy test is also used to evaluate the performance of the new image segmentation algorithm. The threshold variance to mean ratio method was

implemented in the baseline automatic fingerprint identification system, in addition to the "contract and stretch" method for contrast stretching, and simulated test runs were performed. The overall matching accuracy results have improved for DB #1, DB #2 and DB #3. They are shown in Table 4.2 below.

Table 4.2 – Matching Results (Contrast Stretching + Image Segmentation Improved)

	Fingerprint DB #1	**Fingerprint DB #2**	**Fingerprint DB #3**
Pseudo-Spectrum Fusion	85%	88.75%	93.75%

4.3 Image Enhancement Results

Examples of actual fingerprint images before and after improved image enhancement are shown in Figure 4.3 below. The top row in the figure contains the original images and the bottom row contains the images after being exposed to:

1. Contrast stretching using the "contract and stretch" method,
2. Local histogram equalization with image segmentation using the "variance to mean ratio" method,
3. Local normalization using the method from the baseline system and
4. Image morphology using the method from the baseline system

Figure 4.3 – Four Stages of Image Enhancement Examples (Improved)

CHAPTER 5

FEATURE EXTRACTION AND FUSION IMPROVEMENTS

Details for the modification performed on the feature extraction and fusion stage of the baseline automatic fingerprint identification system is discussed in this chapter. The new algorithm description is again followed by a performance evaluation for justification.

5.1 Direction Image

The following quantization algorithm forces the ridge direction estimates in the direction image to one of four angle values, which is an improvement over the un-quantized ridge direction estimates found in the baseline system. The idea behind quantizing the ridge direction estimates stems from the "spatial domain" approach discussed in [12] where each estimate was quantized to one of eight angle values.

5.1.1 Algorithm Description

Yet another mathematical model may be used to represent fingerprint ridge direction and is similar to the one shown in Figure 2.11. It is known as a "quantized orientation field" and is shown in the Cartesian plane in Figure 5.1 below.

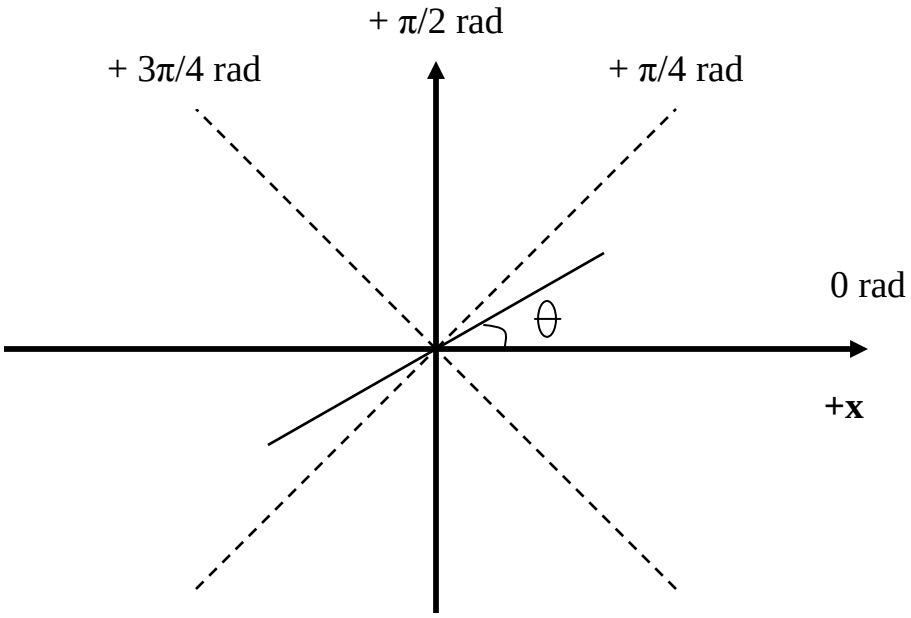

Figure 5.1 – Orientation Field Model (Quantized)

As before, the angle θ represents the orientation of a straight line. The angle θ is similar to the angle described in the vector field model and orientation field model shown in Figure 2.10 and Figure 2.11, respectively, because it is also measured in radians with respect to the positive x-axis (or positive horizontal axis). However, its range is strictly quantized to values of 0, π/4, π/2 and 3π/4 radians with no change in the angle θ when phase-shifted by integer multiples of π radians [12].

This new algorithm takes a ridge direction estimate generated via the Discrete Fourier Transform approach described in Section 2.3.2.6 and quantizes it using the following equation:

$$\theta_{quantized} = \begin{cases} 0 & 0 \le \theta < \pi/8, 7\pi/8 \le \theta < \pi \\ \pi/4 & \pi/8 \le \theta < 3\pi/8 \\ \pi/2 & 3\pi/8 \le \theta < 5\pi/8 \\ 3\pi/4 & 5\pi/8 \le \theta < 7\pi/8 \end{cases} \quad (5.1)$$

The process is repeated until all ridge direction estimates in a given direction image have been quantized.

5.1.2 Performance Evaluation

The quantized ridge direction representation shown in Figure 5.1 demonstrates satisfaction of the requirement for a direction image that reduces noise in the direction estimates. As visual evidence in favor of the new algorithm, the direction image example provided in the next section of this chapter appears to have much smoother transitions between changing ridge directions indicating noise has been reduced or eliminated.

A matching accuracy test is used to evaluate the performance of the new quantized ridge direction algorithm. The quantized direction image was implemented in the baseline automatic fingerprint identification system, in addition to the image enhancement improvements discussed in Chapter 4, and simulated test runs were performed. The overall matching accuracy results have improved for DB #1 and DB #2 and remain unchanged for DB #3. They are shown in Table 5.1 below.

Table 5.1 – Matching Results (Contrast Stretching, Image Seg. + Dir. Image Improved)

	Fingerprint DB #1	**Fingerprint DB #2**	**Fingerprint DB #3**
Pseudo-Spectrum Fusion	86.25%	90%	93.75%

5.2 Direction Image Results

Figure 5.2 provides two examples of actual fingerprints with their associated direction image before and after improvement in the same row. The direction images were estimated using the Discrete Fourier Transform approach discussed in Section 2.3.2.7 of Chapter 2 followed by quantization of the ridge direction estimates.

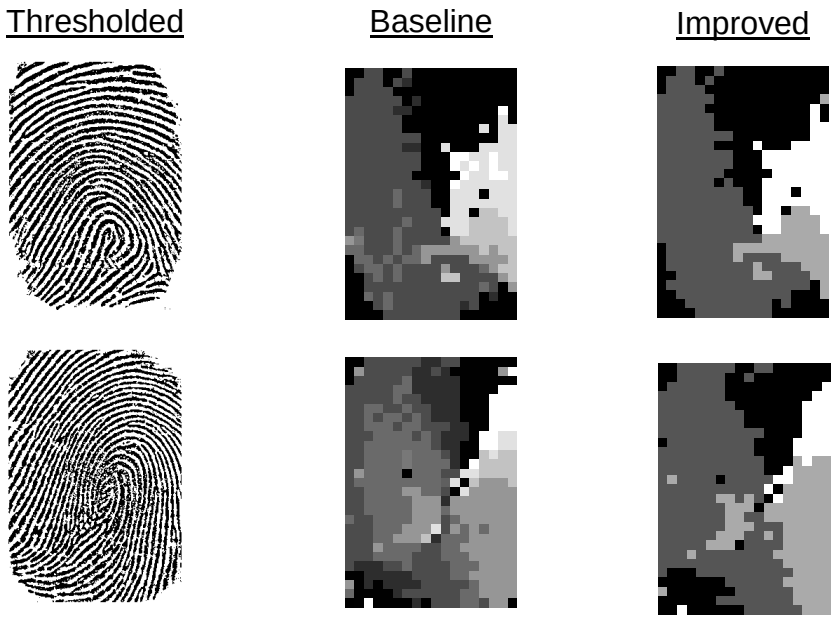

Figure 5.2 – Direction Image Examples (Improved)

CHAPTER 6

ALTERNATIVE CORRELATION-BASED MATCHING SCHEMES

Five alternative correlation-based matching schemes are provided in this chapter, which could be used in place of the “fused features” matching scheme present in the baseline automatic fingerprint identification system and described in Section 2.3.3.1 of Chapter 2. A results section containing three-dimensional correlation-based matching plots follows the descriptions of the alternative matching schemes in order to evaluate performance.

6.1 Direction Feature Only Matching

The proceeding correlation-based matching scheme determines the significance of $\theta(m,n)$.

The direction image only matching process is performed with the following steps:

1. A high-quality fingerprint image from each class in a given database is chosen to become a template image. Each of these selected images is enhanced followed by feature extraction of the direction image only. The direction features from each selected fingerprint image are saved into a template image and stored in a template database. Each is denoted as F_{Tp-Dir}, where p represents the template class.
2. Next, an input fingerprint image is selected from the same given database. It is enhanced followed by feature extraction of the direction image only. The direction features from the input fingerprint image are saved into an input features image and denoted as F_{In-Dir}, where n represents the input fingerprint class.
3. Cross-correlation is then performed on the first template image and input features image using the following equation:

$$C_{Dir}(m,n) = \sum_{l=0}^{N-1}\sum_{k=0}^{M-1} F_{In-Dir}(k,l)F_{Tp-Dir}{}^{*}(k+m,l+n) \qquad -M \le m \le M,$$

$$-N \le n \le N \tag{6.1}$$

4. The resulting cross-correlation matrix contains complex coefficients due to the complex nature of the direction features in F_{Tp-Dir} and F_{In-Dir}. Only the real part of the cross-correlation coefficients is considered when determining the degree of similarity between the template image and input features image. Large, real-valued correlation coefficients indicate a high degree of similarity between the two feature images where as small, real-valued correlation coefficients imply the two images are not at all alike.
5. The same input features image is then cross-correlated with each of the remaining template images stored in the template database. A match is determined by comparing the real-valued coefficients from each cross-correlation matrix with the rest and choosing the one with the largest, real-valued coefficient. For example, if the largest, real-valued cross-correlation coefficient results from crossing the input features image with template image p, then the input features image is considered to match with finger p. A correct match results when p is equal to n.
6. The process described in Step 2 – Step 5 is then repeated for all input features images obtained from the given database. This assigns a template image class to every input features image [12].

6.2 Density Feature Only Matching

The following correlation-based matching scheme determines the significance of $D(m,n)$.

The density image only matching process is performed with the following steps:

1. A high-quality fingerprint image from each class in a given database is chosen to become a template image. Each of these selected images is enhanced followed by feature extraction of the density image only. The density features from each selected fingerprint image are saved into a template image and stored in a template database. Each is denoted as F_{Tp-Den}, where p represents the template class.

2. Next, an input fingerprint image is selected from the same given database. It is enhanced followed by feature extraction of the density image only. The density features from the input fingerprint image are saved into an input features image and denoted as F_{In-Den}, where n represents the input fingerprint class.

3. Cross-correlation is then performed on the first template image and input features image using the following equation:

$$C_{Den}(m,n) = \sum_{l=0}^{N-1}\sum_{k=0}^{M-1} F_{In-Den}(k,l) F_{Tp-Den}{}^{*}(k+m, l+n) \qquad -M \le m \le M,$$

$$-N \le n \le N \tag{6.2}$$

4. The resulting cross-correlation matrix contains only real-valued coefficients due to the nature of the density features in F_{Tp-Den} and F_{In-Den}. Large, real-valued correlation coefficients indicate a high degree of similarity between the two feature images where as small, real-valued correlation coefficients imply the two images are not at all alike.

5. The same input features image is then cross-correlated with each of the remaining template images stored in the template database. A match is determined by comparing the real-valued coefficients from each cross-correlation matrix with the rest and choosing the one with the largest, real-valued coefficient. For example, if the largest, real-valued cross-correlation coefficient results from crossing the input

features image with template image p , then the input features image is considered to match with finger p . A correct match results when p is equal to n .

6. The process described in Step 2 – Step 5 is then repeated for all input features images obtained from the given database. This assigns a template image class to every input features image [12].

6.3 Two Channels with Addition-Type Fusion Matching

The following correlation-based matching scheme uses two channels to compare the direction images and density images separately with addition-type fusion in an attempt to improve matching accuracy.

The weighting factors used when adding the two channels together were selected as those that resulted in the greatest matching accuracy during "trial and error" test runs. The weighting factor, α, was tested ranging from 0.1 to 1.0 in increments of 0.1 and all combinations were applied to the direction correlation coefficients matrix and the density correlation coefficients matrix. The final value for α was chosen to be 0.1.

The two channels with addition matching process is performed with the following steps:

1. A high-quality fingerprint image from each class in a given database is chosen to become a template image. Each of these selected images is enhanced followed by feature extraction of the direction image and density image separately. The direction features and density features from each selected fingerprint image are saved into two template images and stored in a template database. Each pair is denoted as F_{Tp-Dir} and F_{Tp-Den} , where p represents the template class.
2. Next, an input fingerprint image is selected from the same given database. It is enhanced followed by feature extraction of the direction image and density image

separately. The direction features and density features from the input fingerprint image are saved into two input features images and denoted as F_{In-Dir} and F_{In-Den}, where n represents the input fingerprint class.

3. Cross-correlation is then performed on the first template direction image and input features direction image using Equation 6.1. After that, cross-correlation is performed on the first template density image and input features direction image using Equation 6.2. Once the two correlation coefficients matrices are generated, the additive cross-correlation coefficients matrix is created using the following equation:

$$C_{Add}(m,n) = C_{Dir}(m,n) + \alpha \cdot C_{Den}(m,n) \quad -M \le m \le M,\ -N \le n \le N \tag{6.3}$$

4. The resulting cross-correlation matrix contains complex coefficients due to the complex nature of the direction features in F_{Tp-Dir} and F_{In-Dir}. Only the real part of the cross-correlation coefficients is considered when determining the degree of similarity between the template image and input features image. Large, real-valued correlation coefficients indicate a high degree of similarity between the two feature images where as small, real-valued correlation coefficients imply the two images are not at all alike.
5. The same input features image is then cross-correlated with each of the remaining template images stored in the template database. A match is determined by comparing the real-valued coefficients from each additive cross-correlation matrix, $C_{Add}(m,n)$, with the rest and choosing the one with the largest, real-valued coefficient. For example, if the largest, real-valued cross-correlation coefficient results from crossing the input features image with template image p, then the input

features image is considered to match with finger p. A correct match results when p is equal to n.

6. The process described in Step 2 – Step 5 is then repeated for all input features images obtained from the given database. This assigns a template image class to every input features image [12].

6.4 Two Channels with Multiplication-Type Fusion Matching

The following correlation-based matching scheme uses two channels to compare the direction images and density images separately with multiplication-type fusion in an attempt to improve matching accuracy.

The two channels with multiplication matching process is performed with the following steps:

1. A high-quality fingerprint image from each class in a given database is chosen to become a template image. Each of these selected images is enhanced followed by feature extraction of the direction image and density image separately. The direction features and density features from each selected fingerprint image are saved into two template images and stored in a template database. Each pair is denoted as F_{Tp-Dir} and F_{Tp-Den}, where p represents the template class.
2. Next, an input fingerprint image is selected from the same given database. It is enhanced followed by feature extraction of the direction image and density image separately. The direction features and density features from the input fingerprint image are saved into two input features images and denoted as F_{In-Dir} and F_{In-Den}, where n represents the input fingerprint class.
3. Cross-correlation is then performed on the first template direction image and input features direction image using Equation 6.1. After that, cross-correlation is

performed on the first template density image and input features direction image using Equation 6.2. Once the two correlation coefficients matrices are generated, the multiplicative cross-correlation coefficients matrix is created using the following equation:

$$C_{Mult}(m,n) = C_{Dir}(m,n) \cdot C_{Den}(m,n) \qquad -M \le m \le M,\ -N \le n \le N \tag{6.4}$$

4. The resulting cross-correlation matrix contains complex coefficients due to the complex nature of the direction features in F_{Tp-Dir} and F_{In-Dir}. Only the real part of the cross-correlation coefficients is considered when determining the degree of similarity between the template image and input features image. Large, real-valued correlation coefficients indicate a high degree of similarity between the two feature images where as small, real-valued correlation coefficients imply the two images are not at all alike.
5. The same input features image is then cross-correlated with each of the remaining template images stored in the template database. A match is determined by comparing the real-valued coefficients from each multiplicative cross-correlation matrix, $C_{Mult}(m,n)$, with the rest and choosing the one with the largest, real-valued coefficient. For example, if the largest, real-valued cross-correlation coefficient results from crossing the input features image with template image p, then the input features image is considered to match with finger p. A correct match results when p is equal to n.
6. The process described in Step 2 – Step 5 is then repeated for all input features images obtained from the given database. This assigns a template image class to every input features image [12].

6.5 Two Templates per Class Matching

The following correlation-based matching scheme uses the Pseudo Spectrum Fusion approach with two templates per class in an attempt to improve matching accuracy.

The two templates per class matching process is performed using the following steps:

1. Two high-quality fingerprint images from each class in a given database is chosen to become template images. Each of these selected images is enhanced followed by feature extraction and fusion of the direction image and density image. The two sets of fused features from each selected fingerprint image are saved into two template images per class and stored in a template database. Each pair is denoted as F_{Tp1} and F_{Tp2}, where p represents the template class.
2. Next, an input fingerprint image is selected from the same given database. It is enhanced followed by feature extraction and fusion of the direction image and density image. The fused features from the input fingerprint image are saved into an input features images and denoted as F_{In}, where n represents the input fingerprint class.
3. Cross-correlation is then performed on the first template image and input features image using this equation:

$$C_{TT1}(m,n) = \sum_{l=0}^{N-1}\sum_{k=0}^{M-1} F_{In}(k,l)F_{Tp1}{}^{*}(k+m,l+n) \qquad -M \le m \le M,\ -N \le n \le N \tag{6.5}$$

After that, cross-correlation is performed on the second template image and input features image using this equation:

$$C_{TT2}(m,n) = \sum_{l=0}^{N-1}\sum_{k=0}^{M-1} F_{In}(k,l)F_{Tp2}{}^{*}(k+m,l+n) \qquad -M \le m \le M,\ -N \le n \le N$$

(6.6)

Once the two correlation coefficients matrices are generated, the two templates maximum cross-correlation coefficients matrix is created using the following equation:

$$C_{Max}(m,n) = \begin{cases} C_{TT1}(m,n) & \max\{\mathrm{Re}\{C_{TT1}(m,n)\}\} > \max\{\mathrm{Re}\{C_{TT2}(m,n)\}\} \\ C_{TT2}(m,n) & \max\{\mathrm{Re}\{C_{TT1}(m,n)\}\} \le \max\{\mathrm{Re}\{C_{TT2}(m,n)\}\} \end{cases}$$

$$-M \le m \le M,\ -N \le n \le N \qquad (6.7)$$

4. The resulting cross-correlation matrix contains complex coefficients due to the complex nature of the fused features in F_{Tp1}, F_{Tp2} and F_{In}. Only the real part of the cross-correlation coefficients is considered when determining the degree of similarity between the template image and input features image. Large, real-valued correlation coefficients indicate a high degree of similarity between the two feature images where as small, real-valued correlation coefficients imply the two images are not at all alike.
5. The same input features image is then cross-correlated with each of the remaining template image pairs stored in the template database. A match is determined by comparing the real-valued coefficients from each maximum cross-correlation matrix, $C_{Max}(m,n)$, with the rest and choosing the one with the largest, real-valued coefficient. For example, if the largest, real-valued cross-correlation coefficient results from crossing the input features image with template image set p, then the input features image is considered to match with finger p. A correct match results when p is equal to n.

6. The process described in Step 2 – Step 5 is then repeated for all input features images obtained from the given database. This assigns a template image set class to every input features image [12].

6.6 Correlation-Based Matching Results

The following examples in Figure 6.1 – Figure 6.9 provide a visual demonstration of the "correlation-based" matching schemes covered in the previous sections of this chapter. Three correlation-based matching scenarios are presented and they include:

1. Two identical images,
2. Two different images from the same fingerprint class and
3. Two different images from different fingerprint classes

For each scenario, the real-valued cross-correlation coefficients matrices are shown in three-dimensional mesh grid plots using these three types of approaches with all improvements from Chapter 4 and Chapter 5 incorporated:

1. Single Feature Matching,
2. Two Channels Features Matching and
3. Fused Features Matching

The fingerprint images used as the template image and input features image in the examples are shown above the three-dimensional mesh grid plots for reference [12].

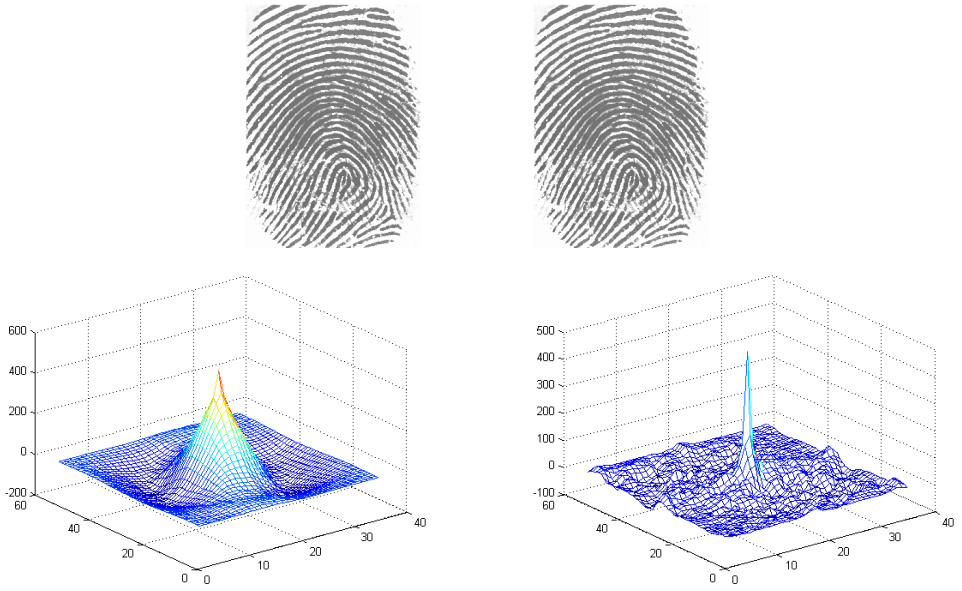

Direction Feature Only

Density Feature Only

Figure 6.1 – Single Feature Matching: Exact Same Images

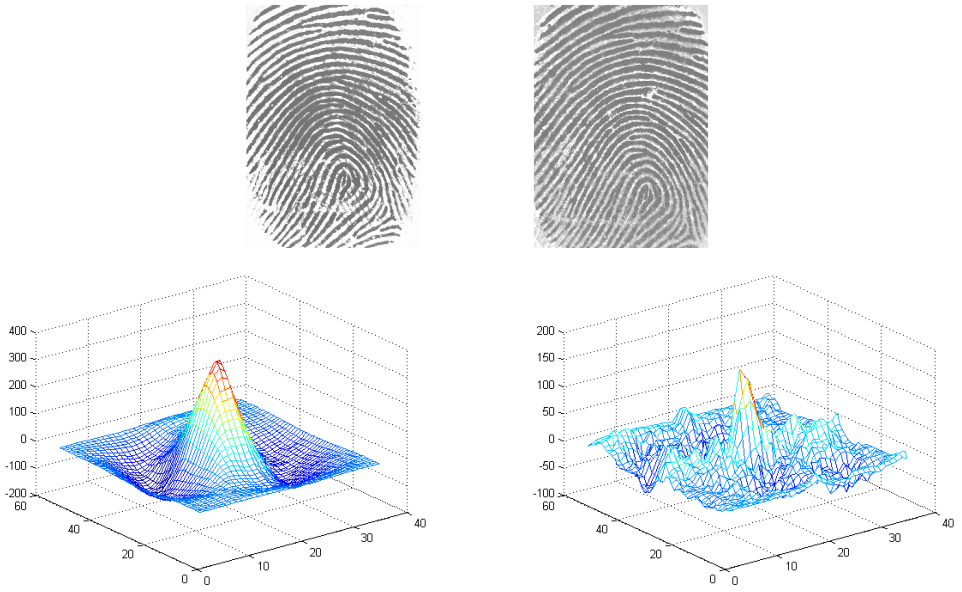

Direction Feature Only

Density Feature Only

Figure 6.2 – Single Feature Matching: Different Images from Same Class

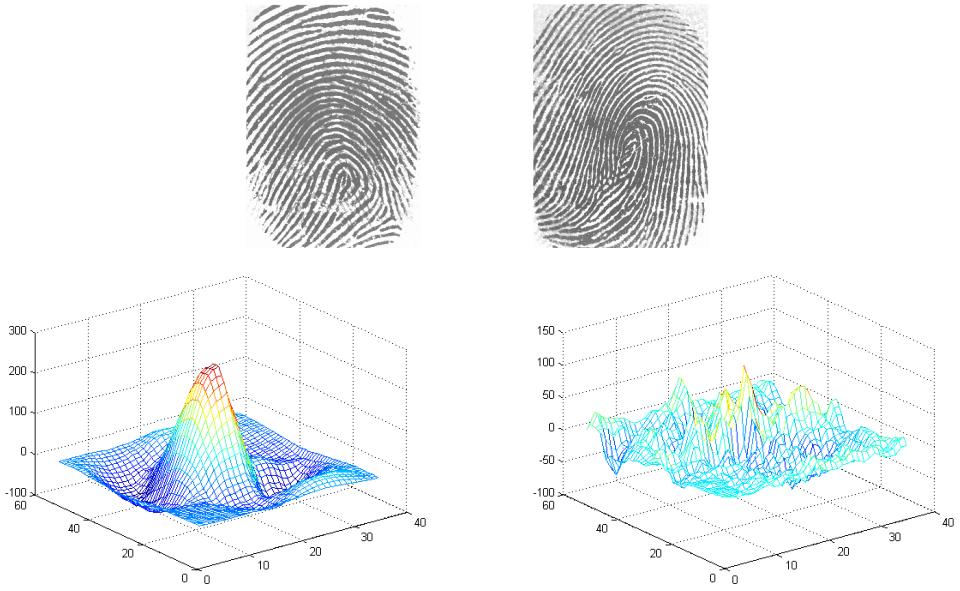

Direction Feature Only

Density Feature Only

Figure 6.3 – Single Feature Matching: Different Images from Different Classes

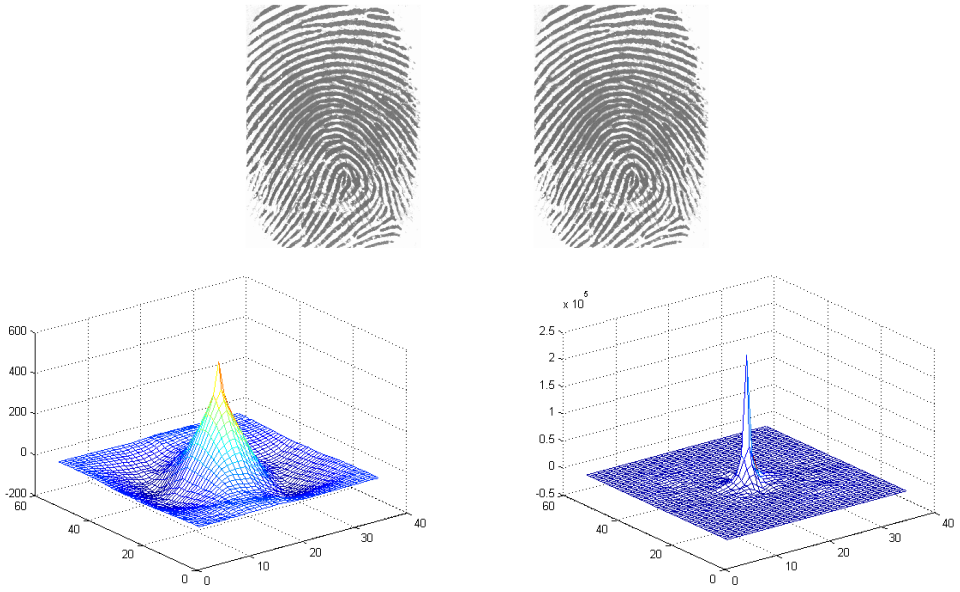

Two Channels with
Addition-Type Fusion

Two Channels with
Multiplication-Type Fusion

Figure 6.4 – Two Channels Features Matching: Exact Same Images

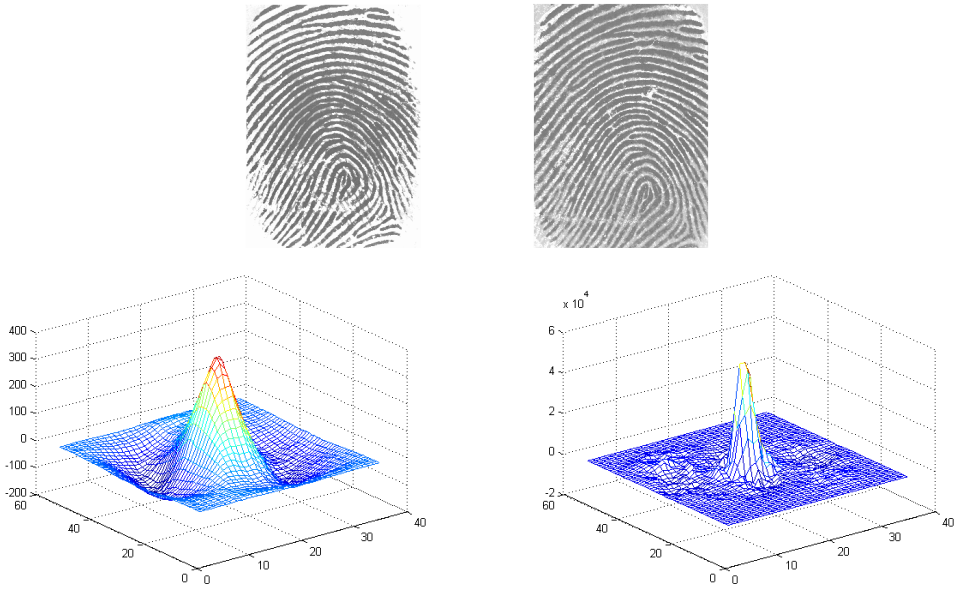

Two Channels with
Addition-Type Fusion

Two Channels with
Multiplication-Type Fusion

Figure 6.5 –Two Channels Features Matching: Different Images from Same Class

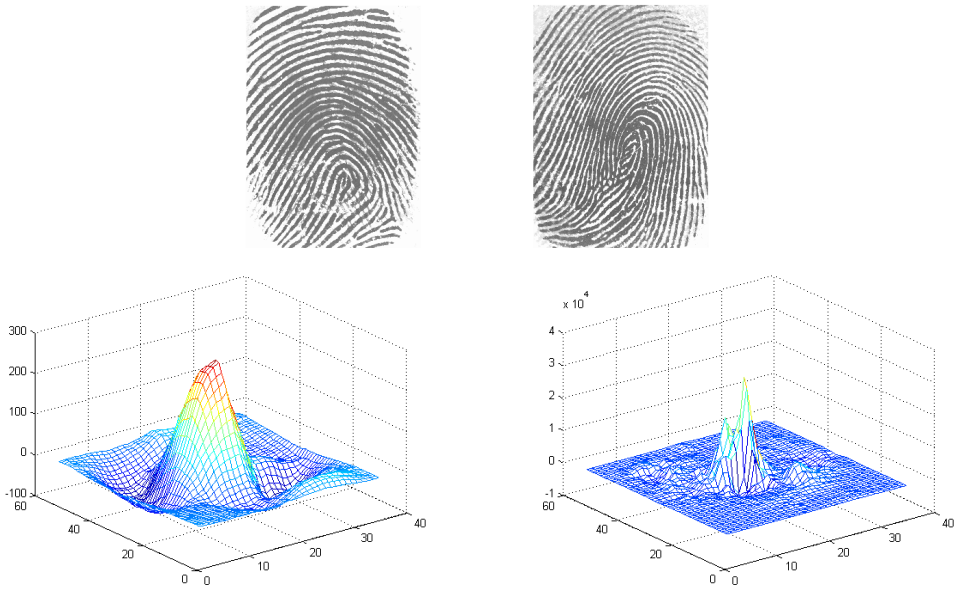

Two Channels with
Addition-Type Fusion

Two Channels with
Multiplication-Type Fusion

Figure 6.6 – Two Channels Features Matching: Different Images from Different Classes

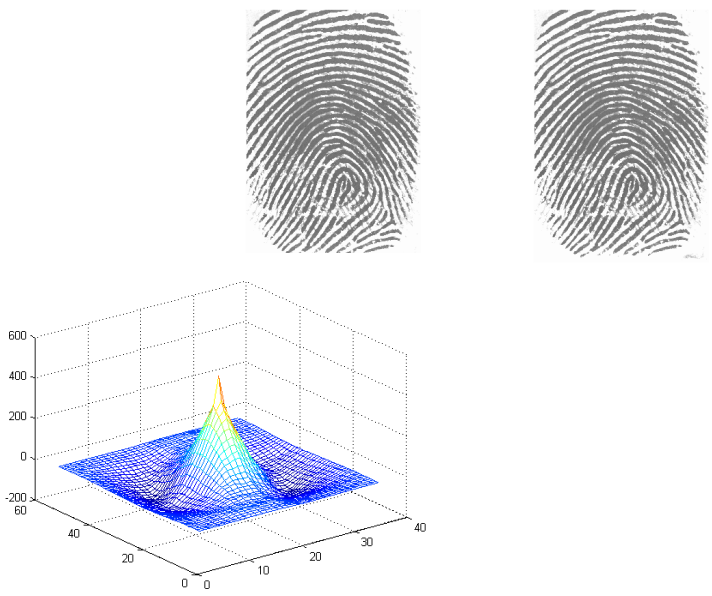

Pseudo Spectrum Fusion

Figure 6.7 – Fused Features Matching: Exact Same Images

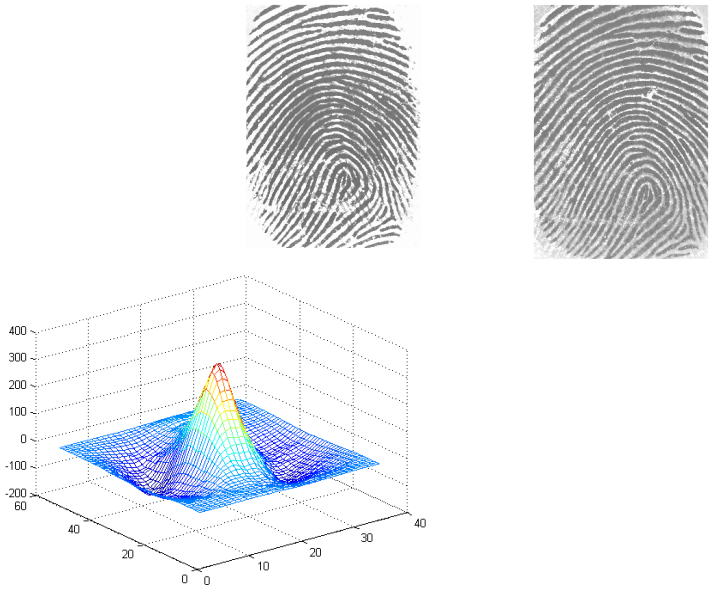

Pseudo Spectrum Fusion

Figure 6.8 – Fused Features Matching: Different Images from Same Class

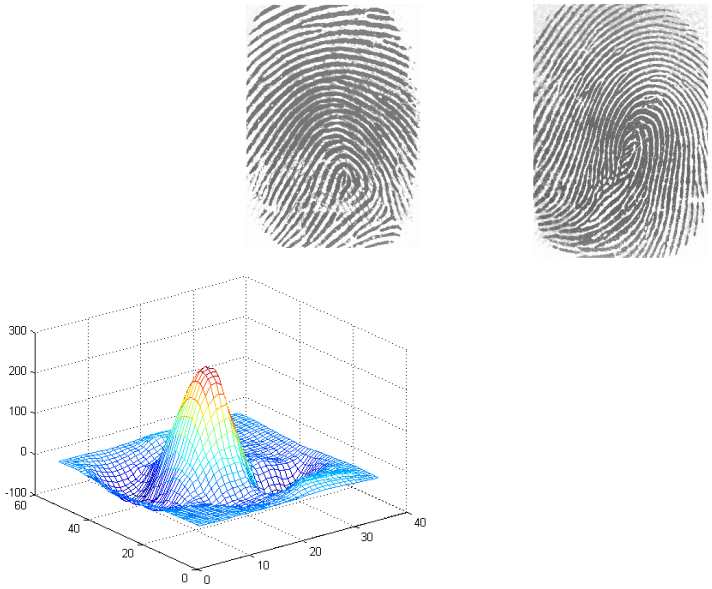

Pseudo Spectrum Fusion

Figure 6.9 – Fused Features Matching: Different Images from Different Classes

The examples shown in Figure 6.1 - Figure 6.9 once again verify that correlation-based matching schemes work. When the two fingerprint images are a correct match, as in Figure 6.1, Figure 6.2, Figure 6.4, Figure 6.5, Figure 6.7 and Figure 6.8, large, real-valued cross-correlation coefficients are associated with the three-dimensional mesh grid plots. The visual indicator for this is the large peak in any one of the plots shown in Figure 6.1, Figure 6.2, Figure 6.4, Figure 6.5, Figure 6.7 and Figure 6.8. For the two fingerprint images that belong to separate classes in Figure 6.3, Figure 6.6 and Figure 6.9, the real-valued cross-correlation coefficients are smaller which indicates a non-match. The visual indicator for this is a much smaller peak in either of the three-dimensional mesh grid plots shown in Figure 6.3, Figure 6.6 and Figure 6.9 [12].

CHAPTER 7

SIMULATION EXPERIMENT RESULTS

This chapter presents a matching simulation experiment using the alternative matching schemes discussed in Chapter 7. The Pseudo Spectrum Fusion approach from the baseline fingerprint identification system is also included. The image enhancement improvements in Chapter 4 and feature extraction and fusion improvement in Chapter 5 are incorporated in these simulation experiments to provide the best possible matching accuracy.

7.1 Objectives

The experiments in this chapter are conducted in order to validate the effectiveness of using ridge direction and ridge density as unique features in conjunction with various correlation-based matching schemes in an automatic fingerprint identification system. This type of testing also evaluates the performance of the Discrete Fourier Transform approach since it is used to estimate the ridge direction and ridge density. The fully-functional automatic fingerprint identification system featured in this experiment includes the baseline automatic fingerprint identification system covered in Chapter 2, along with image enhancement improvements, feature extraction and fusion improvement and alternative matching schemes discussed in Chapter 4, Chapter 5 and Chapter 6, respectively. Actual human fingerprint images are matched against stored template images in a database and the results are summarized in tables in the final section of this chapter [12].

7.2 Fingerprint Database Description

The three fingerprint databases used in this simulation experiment were obtained from Fingerprint Verification Competition 2000 (or FVC2000) [27]. Each database contains exactly 80 fingerprint images and they comprise a total of 10 different classes or fingers. In other words, the databases are 10 fingers wide by eight impressions deep. No fingerprint images from the same class are exactly alike. The fingerprint images in Database #1 are of size 300x300 pixels and were captured on a 500 dpi "Secure Desktop Scanner" low-cost optical sensor. Database #2 contains images of size 256x364 pixels collected from a 500 dpi "Touch Chip" low-cost capacitive sensor. Finally, the images that make up Database #3 are 448x478 pixels in size and were captured from a 500 dpi "DF-90" optical sensor [28].

7.3 Experiment Setup

There are six separate matching schemes run on the three fingerprint image databases described in the previous section of this chapter. Matching Scheme #1 is Direction Only Features which uses a single extracted feature via the Discrete Fourier Transform approach. In Matching Scheme #2, Density Only Features also uses a single extracted feature via the Discrete Fourier Transform approach. Matching Scheme #3 is Two Channels with Addition-Type Fusion which uses both extracted features in two separate channels via the Discrete Fourier Transform approach. Matching Scheme #4 is Two Channels with Multiplication-Type Fusion which uses both extracted features in two separate channels via the Discrete Fourier Transform approach. In Matching Scheme #5, Pseudo Spectrum Fusion uses a fused form of both extracted features via the Discrete Fourier Transform approach. Matching Scheme #6 is Two Templates per Class which uses a fused form of both extracted features via the Discrete Fourier Transform approach and includes a second template image for each class of fingerprint [12].

Before the six matching schemes are run in the experiment, there are two databases of template images which must be generated for fingerprint image Database #1. In the cases of Matching Scheme #1 – Matching Scheme #5, which use the Discrete Fourier Transform approach, the highest quality image from each of the 10 classes is chosen, enhanced, and then a set of features is extracted, fused and stored in 10 template images. Matching Scheme #6 uses the Discrete Fourier Transform approach, but with two templates per class, so the two highest quality images from each of the 10 classes are chosen, enhanced, and then a set of features is extracted, fused and stored in 20 template images [12].

Once the template image databases are generated for the six matching schemes, each of the 80 test images in fingerprint Database #1 are matched against 10 template images using Direction Features Only in Matching Scheme #1. The matching results contain a total of 800 matches for fingerprint Database #1 and are collected and analyzed to determine correct matches and incorrect matches. Then, the 80 test images in fingerprint Database #1 are matched against 10 template images for Matching Scheme #2 – Matching Scheme #5. In each case, the 800 total matches for fingerprint Database #1 are collected and analyzed to determine correct and incorrect matches. Finally, the 80 test images in fingerprint Database #1 are matched against 20 template images for Two Templates per Class in Matching Scheme #6. This still results in 800 total matches for fingerprint Database #1 that are collected and analyzed to determine correct and incorrect matches. After the six matching schemes are performed using fingerprint Database #1, they are repeated the same way using fingerprint Database #2 and fingerprint Database #3 [12].

7.4 Data Formatting Description

The matching data results from the six matching schemes are displayed in 18 tables shown in the next section. One of the six matching schemes is run on fingerprint Database #1, fingerprint Database #2 or fingerprint Database #3 per table. Each of the 18 tables contains test fingerprint image labels along the leftmost column and template image labels along the topmost row. The test fingerprint images are represented as F_{In}, where n denotes the input fingerprint class, which falls in the range of one to 10. Similarly, the template images are represented as F_{Tp}, where p denotes the template class and is once again between one and 10. A raw data value x in any one of the table cells represents the number of test images from finger n that have been matched with template p. The values for n and p are located by viewing the corresponding labels showing the input image subscript on the leftmost column and the corresponding template image subscript on the topmost row of the matching results table. Since there are eight impressions per class of fingerprint image per database, each row in a data table always contains raw data values that total eight fingerprint images. The raw data values appearing along the diagonal (i.e. cell numbers (1,1), (2,2), (3,3), …, (10,10)) indicate the number of correct matches per class. Raw data values appearing in all other cell locations in the matching results tables are incorrect matches [12].

7.5 Matching Data Results

Matching results data for each of the six matching schemes in this experiment is shown in matching data tables in this section. Table 7.1 - Table 7.6 contain matching results data obtained from performing Matching Scheme #1 – Matching Scheme #6 on fingerprint Database #1, respectively. Following that, Table 7.7 - Table 7.12 show the results from running Matching Scheme #1 – Matching Scheme #6 on fingerprint

Database #2. The next three tables, which are Table 7.13 - Table 7.18, contain the results from performing the same six matching schemes, but this time using fingerprint Database #3. Table 7.19 is the final table and it displays a summary of the overall matching accuracy of the six matching schemes covered in this thesis [12].

Using matching results data, the six matching schemes are ranked in order of matching accuracy from lowest to highest. The Density Only Feature matching scheme is seen performing with the lowest matching accuracy in Tables 7.2, 7.8 and 7.14. When comparing fingerprint images, it should be noted that the ridge density is not nearly as unique as the ridge direction and thus a density only matching scheme is a very poor performer. This is followed by the Two Channels with Multiplication-Type Fusion scheme that was not much better with results shown in Tables 7.4, 7.10 and 7.16. Multiplying the highly-unique ridge direction features with ridge density features vastly degraded their performance. The Direction Only Feature and Two Channels with Addition-Type Fusion matching schemes were similar in matching accuracy which was much better than the first two matching schemes mentioned. Their similar matching performance is due to scaling of the ridge density by a factor of 0.10 so that it had a minimal impact on the direction and density features sum in the Two Channels with Addition-Type Fusion matching scheme. Their results are displayed in Tables 7.1, 7.7 and 7.13 and Tables 7.3, 7.9 and 7.15, respectively. The Pseudo Spectrum Fusion matching scheme exhibited quite an impressive matching accuracy in comparison to those previously mentioned with its results shown in Tables 7.5, 7.11 and 7.17. Pseudo Spectrum Fusion creates a feature which is unique beyond what is accomplished using the ridge direction or ridge density as separate features. Therefore, its matching performance exceeds all of the previously mentioned matching schemes. Last of all, Two Templates per Class, which uses Pseudo Spectrum fused features in its matching scheme, resulted in a

matching accuracy which is higher than any of the others previously mentioned. Combining the advantage of a very unique feature with the ability to correctly match a lower quality fingerprint image using a second, lower quality template image makes this matching scheme outperform all others. Its results can be seen in Tables 7.6, 7.12 and 7.18. The Two Templates per Class matching scheme is chosen as the preferred matching scheme in the automatic fingerprint identification system in this thesis.

Table 7.1 – Direction Feature Only Matching (Database #1)

Input Images	**Direction Feature Only Template Images**										**Matching %**
	F_{T1}	F_{T2}	F_{T3}	F_{T4}	F_{T5}	F_{T6}	F_{T7}	F_{T8}	F_{T9}	F_{T10}	
F_{I1}	8										100%
F_{I2}		8									100%
F_{I3}			8								100%
F_{I4}				8							100%
F_{I5}					6		2				75%
F_{I6}						8					100%
F_{I7}	1						7				87.5%
F_{I8}		1						7			87.5%
F_{I9}					3				5		62.5%
F_{I10}	4	1								3	37.5%

Table 7.2 – Density Feature Only Matching (Database #1)

Input Images	Density Feature Only Template Images										Matching %
	F_{T1}	F_{T2}	F_{T3}	F_{T4}	F_{T5}	F_{T6}	F_{T7}	F_{T8}	F_{T9}	F_{T10}	
F_{I1}	3	3				1	1				37.5%
F_{I2}		4			2		2				50%
F_{I3}			5		1			2			62.5%
F_{I4}		2	1	4	1						50%
F_{I5}					6	1	1				75%
F_{I6}						7		1			87.5%
F_{I7}						1	7				87.5%
F_{I8}					1	5	1	1			12.5%
F_{I9}					2	1		1	4		50%
F_{I10}						4			1	3	37.5%

Table 7.3 – Two Channels with Addition-Type Fusion Matching (Database #1)

Input Images	Two Channels with Addition-Type Fusion Template Images										Matching %
	F_{T1}	F_{T2}	F_{T3}	F_{T4}	F_{T5}	F_{T6}	F_{T7}	F_{T8}	F_{T9}	F_{T10}	
F_{I1}	8										100%
F_{I2}		8									100%
F_{I3}			8								100%
F_{I4}				8							100%
F_{I5}					6		2				75%
F_{I6}						8					100%
F_{I7}	1						7				87.5%
F_{I8}		1						7			87.5%
F_{I9}					3				5		62.5%
F_{I10}	4	1								3	37.5%

Table 7.4 – Two Channels with Multiplication-Type Fusion Matching (Database #1)

Input Images	Two Channels with Multiplication Fusion Template Images										Matching %
	F_{T1}	F_{T2}	F_{T3}	F_{T4}	F_{T5}	F_{T6}	F_{T7}	F_{T8}	F_{T9}	F_{T10}	
F_{I1}	7						1				87.5%
F_{I2}		7				1					87.5%
F_{I3}		1	7								87.5%
F_{I4}				5	1		2				62.5%
F_{I5}					4		3	1			50%
F_{I6}						7		1			87.5%
F_{I7}					1		7				87.5%
F_{I8}		3				2		3			37.5%
F_{I9}					3				5		62.5%
F_{I10}	1	1				1		1		4	50%

Table 7.5 – Pseudo Spectrum Fusion Matching (Database #1)

Input Images	Pseudo Spectrum Fusion Template Images										Matching %
	F_{T1}	F_{T2}	F_{T3}	F_{T4}	F_{T5}	F_{T6}	F_{T7}	F_{T8}	F_{T9}	F_{T10}	
F_{I1}	8										100%
F_{I2}		8									100%
F_{I3}			8								100%
F_{I4}				8							100%
F_{I5}				1	6		1				75%
F_{I6}						8					100%
F_{I7}							8				100%
F_{I8}		2						6			75%
F_{I9}					3				5		62.5%
F_{I10}	3	1								4	50%

Table 7.6 – Two Templates per Class Matching (Database #1)

Input Images	Two Templates per Class Template Images										Matching %
	F_{T1}	F_{T2}	F_{T3}	F_{T4}	F_{T5}	F_{T6}	F_{T7}	F_{T8}	F_{T9}	F_{T10}	
F_{I1}	8										100%
F_{I2}		8									100%
F_{I3}			8								100%
F_{I4}				8							100%
F_{I5}					6				2		75%
F_{I6}						8					100%
F_{I7}							8				100%
F_{I8}		1				1		6			75%
F_{I9}					1				7		87.5%
F_{I10}	1	1								6	75%

Table 7.7 – Direction Feature Only Matching (Database #2)

Input Images	Direction Feature Only Template Images										Matching %
	F_{T1}	F_{T2}	F_{T3}	F_{T4}	F_{T5}	F_{T6}	F_{T7}	F_{T8}	F_{T9}	F_{T10}	
F_{I1}	8										100%
F_{I2}		7						1			87.5%
F_{I3}			8								100%
F_{I4}				8							100%
F_{I5}					4		3			1	50%
F_{I6}						8					100%
F_{I7}							8				100%
F_{I8}		2				2		4			50%
F_{I9}									8		100%
F_{I10}	1								1	6	75%

Table 7.8 – Density Feature Only Matching (Database #2)

Input Images	Density Feature Only Template Images										Matching %
	F_{T1}	F_{T2}	F_{T3}	F_{T4}	F_{T5}	F_{T6}	F_{T7}	F_{T8}	F_{T9}	F_{T10}	
F_{I1}	2	3				1	2				25%
F_{I2}		4				2			2		50%
F_{I3}		1	2			4			1		25%
F_{I4}			1	3		2	1		1		37.5%
F_{I5}		1	3	1	2	1					25%
F_{I6}						6		1	1		75%
F_{I7}				1			7				87.5%
F_{I8}				1				6	1		75%
F_{I9}		1		2		2			3		37.5%
F_{I10}						3				5	62.5%

Table 7.9 – Two Channels with Addition-Type Fusion Matching (Database #2)

Input Images	Two Channels with Addition-Type Fusion Template Images										Matching %
	F_{T1}	F_{T2}	F_{T3}	F_{T4}	F_{T5}	F_{T6}	F_{T7}	F_{T8}	F_{T9}	F_{T10}	
F_{I1}	8										100%
F_{I2}		7							1		87.5%
F_{I3}			8								100%
F_{I4}				8							100%
F_{I5}					4		3			1	50%
F_{I6}						8					100%
F_{I7}							8				100%
F_{I8}		1				2		5			62.5%
F_{I9}					1				7		87.5%
F_{I10}									1	7	87.5%

Table 7.10 – Two Channels with Multiplication-Type Fusion Matching (Database #2)

Input Images	Two Channels with Multiplication Fusion Template Images										Matching %
	F_{T1}	F_{T2}	F_{T3}	F_{T4}	F_{T5}	F_{T6}	F_{T7}	F_{T8}	F_{T9}	F_{T10}	
F_{I1}	5	3									62.5%
F_{I2}		5				2			1		62.5%
F_{I3}		2	5			1					62.5%
F_{I4}		1		6					1		75%
F_{I5}				1	4				2	1	50%
F_{I6}		1				6		1			75%
F_{I7}							8				100%
F_{I8}				1		2		5			62.5%
F_{I9}				1	1				6		75%
F_{I10}										8	100%

Table 7.11 – Pseudo Spectrum Fusion Matching (Database #2)

Input Images	Pseudo Spectrum Fusion Template Images										Matching %
	F_{T1}	F_{T2}	F_{T3}	F_{T4}	F_{T5}	F_{T6}	F_{T7}	F_{T8}	F_{T9}	F_{T10}	
F_{I1}	8										100%
F_{I2}		7					1				87.5%
F_{I3}			8								100%
F_{I4}				8							100%
F_{I5}	1				5		1		1		62.5%
F_{I6}						8					100%
F_{I7}							8				100%
F_{I8}			1			2		4		1	50%
F_{I9}									8		100%
F_{I10}										8	100%

Table 7.12 – Two Templates per Class Matching (Database #2)

Input Images	Two Templates per Class Template Images										Matching %
	F_{T1}	F_{T2}	F_{T3}	F_{T4}	F_{T5}	F_{T6}	F_{T7}	F_{T8}	F_{T9}	F_{T10}	
F_{I1}	8										100%
F_{I2}		8									100%
F_{I3}			8								100%
F_{I4}				8							100%
F_{I5}	1			1	6						75%
F_{I6}						8					100%
F_{I7}							8				100%
F_{I8}		1	2					5			62.5%
F_{I9}									8		100%
F_{I10}										8	100%

Table 7.13 – Direction Feature Only Matching (Database #3)

Input Images	Direction Feature Only Template Images										Matching %
	F_{T1}	F_{T2}	F_{T3}	F_{T4}	F_{T5}	F_{T6}	F_{T7}	F_{T8}	F_{T9}	F_{T10}	
F_{I1}	8										100%
F_{I2}		8									100%
F_{I3}			8								100%
F_{I4}				8							100%
F_{I5}					7					1	87.5%
F_{I6}						8					100%
F_{I7}							8				100%
F_{I8}								8			100%
F_{I9}									8		100%
F_{I10}	1									7	87.5%

Table 7.14 – Density Feature Only Matching (Database #3)

Input Images	Density Feature Only Template Images										Matching %
	F_{T1}	F_{T2}	F_{T3}	F_{T4}	F_{T5}	F_{T6}	F_{T7}	F_{T8}	F_{T9}	F_{T10}	
F_{I1}	4					1				3	50%
F_{I2}	1	1		2		4					12.5%
F_{I3}	2		2			1		3			25%
F_{I4}	1			6		1					75%
F_{I5}	4				2	1	1				25%
F_{I6}	2					4				2	50%
F_{I7}	4						4				50%
F_{I8}						1	1	6			75%
F_{I9}									7	1	87.5%
F_{I10}										8	100%

Table 7.15 – Two Channels with Addition-Type Fusion Matching (Database #3)

Input Images	Two Channels with Addition-Type Fusion Template Images										Matching %
	F_{T1}	F_{T2}	F_{T3}	F_{T4}	F_{T5}	F_{T6}	F_{T7}	F_{T8}	F_{T9}	F_{T10}	
F_{I1}	8										100%
F_{I2}		8									100%
F_{I3}	1		7								87.5%
F_{I4}	1			7							87.5%
F_{I5}					7					1	87.5%
F_{I6}						8					100%
F_{I7}							8				100%
F_{I8}								8			100%
F_{I9}									8		100%
F_{I10}	2									6	75%

Table 7.16 – Two Channels with Multiplication-Type Fusion Matching (Database #3)

Input Images	Two Channels with Multiplication Fusion Template Images										Matching %
	F_{T1}	F_{T2}	F_{T3}	F_{T4}	F_{T5}	F_{T6}	F_{T7}	F_{T8}	F_{T9}	F_{T10}	
F_{I1}	8										100%
F_{I2}		4				4					50%
F_{I3}	3		3	1				1			37.5%
F_{I4}	1			7							87.5%
F_{I5}	2				6						75%
F_{I6}						8					100%
F_{I7}	1						7				87.5%
F_{I8}						1	1	6			75%
F_{I9}									8		100%
F_{I10}	2									6	75%

Table 7.17 – Pseudo Spectrum Fusion Matching (Database #3)

Input Images	Pseudo Spectrum Fusion Template Images										Matching %
	F_{T1}	F_{T2}	F_{T3}	F_{T4}	F_{T5}	F_{T6}	F_{T7}	F_{T8}	F_{T9}	F_{T10}	
F_{I1}	8										100%
F_{I2}		8									100%
F_{I3}			8								100%
F_{I4}	1			7							87.5%
F_{I5}	1				5					2	62.5%
F_{I6}						8					100%
F_{I7}							8				100%
F_{I8}								8			100%
F_{I9}									8		100%
F_{I10}	1									7	87.5%

Table 7.18 – Two Templates per Class Matching (Database #3)

Input Images	Two Templates per Class Template Images										Matching %
	F_{T1}	F_{T2}	F_{T3}	F_{T4}	F_{T5}	F_{T6}	F_{T7}	F_{T8}	F_{T9}	F_{T10}	
F_{I1}	8										100%
F_{I2}		8									100%
F_{I3}			8								100%
F_{I4}				8							100%
F_{I5}	1				6					1	75%
F_{I6}						8					100%
F_{I7}							8				100%
F_{I8}								8			100%
F_{I9}									8		100%
F_{I10}										8	100%

Table 7.19 – Overall Matching Performance Results (Improved)

	Fingerprint DB #1	Fingerprint DB #2	Fingerprint DB #3
Direct Grayscale (Baseline)	68.75%	83.75%	71.25%
Pseudo-Spectrum Fusion (Baseline)	70%	85%	82.5%
Direction Feature Only	85%	86.25%	97.5%
Density Feature Only	55%	50%	55%
Two Channels with Addition-Type Fusion	85%	87.5%	93.75%
Two Channels with Multiplication Fusion	70%	72.5%	78.75%
Pseudo-Spectrum Fusion	86.25%	90%	93.75%
Two Templates per Class	91.25%	93.75%	97.5%

CHAPTER 8

CONCLUSIONS AND FUTURE RESEARCH

Conclusions realized from the research performed in this thesis with suggestions for future research ideas are discussed in this chapter.

8.1 Conclusions of this Thesis

An entire automatic fingerprint identification system has been reviewed and certain components were modified, while others were newly implemented, with the goal of improving overall matching accuracy in this thesis. In summary, the following has been accomplished:

1. The image enhancement stage of the system had certain components modified while others were entirely replaced. The simple transformation contrast stretching was replaced with the “contract and stretch” method for contrast stretching. For image segmentation, the single point foreground/background threshold variance computation was upgraded to a variance to mean ratio. All together, these image enhancement upgrades and replacements not only provide a greater reduction in various types of noise, but also further reduce overall processing time by removing more unnecessary background information.
2. The direction image is upgraded by quantizing the ridge direction estimates into four discrete levels, which were previously un-quantized. This new quantization method helps further reduce noise present in the direction estimates that originated in the fingerprint image.

3. A correlation-based matching scheme is utilized for identifying an input fingerprint image with one of the template images in a stored database using only the direction features. The result is a template class number.
4. A correlation-based matching scheme is utilized for identifying an input fingerprint image with one of the template images in a stored database using only the density features. The result is a template class number.
5. A correlation-based matching scheme is utilized for identifying an input fingerprint image with one of the template images in a stored database using direction and density features in two separate channels. The separate channels are then combined using addition-type fusion. The result is a template class number.
6. A correlation-based matching scheme is utilized for identifying an input fingerprint image with one of the template images in a stored database using direction and density features in two separate channels. The separate channels are then combined using multiplication-type fusion. The result is a template class number.
7. A correlation-based matching scheme is utilized for identifying an input fingerprint image with one of the template images in a stored database containing two templates per class using Pseudo Spectrum fused direction and density features. The result is a template class number.

8.2 Recommended Future Research

The automatic fingerprint identification system covered in this thesis has been improved via updates to existing algorithms and also implementation of new ones. In hopes to improve the existing technology beyond the scope of this thesis, the following are future research ideas that could be explored:

1. Automated routines could be developed for computing the scaling factor, α, that is present in the threshold variance to mean ratio in image segmentation and Two Channels with Addition-Type Fusion matching scheme.
2. The correlation-based matching scheme using two template images per class could be expanded to three or more template images per class. When adding a new template image per class, the trade-off of improved matching accuracy versus increased processing time must be considered.
3. The two-dimensional Discrete Fourier Transform can be applied to the Pseudo Spectrum fused feature, which would result in a new type of feature. This new feature may provide useful information for the automatic fingerprint identification system.

REFERENCES

[1] A.K. Jain, L. Hong and R. Bolle, “An Identity-Authentication System Using Fingerprints,” Proc. IEEE, vol. 85, pp. 1365–1388, Sept. 1997.

[2] R. Kluver, “Globalization, Informatization, and Intercultural Communication,” [Online]. Available: http:/withww.acjournal.org/holdings/vol3/Iss3/spec1/kluver.htm [Accessed: Aug. 23, 2010].

[3] G. Aguilar, G. Sanchez, K. Toscano, M. Salinas, M. Nakano and H. Perez, “Fingerprint Recognition,” *presented at Second International Conference on Internet Monitoring and Protection*, 2007.

[4] D. Corcoran, D. Sims and B. Hillhouse, “Smart Cards and Biometrics: Your Key to PKI,” *Linux Journal*, issue 59, March 1999. [Online]. Available: http:/withww.linuxjournal.com. [Accessed: August 23, 2010].

[5] J.D. Woodward, Jr., N.M. Orlans and P.T. Higgins, “Biometrics”. McGraw-Hill/Osborne, 2003.

[6] S. Prabhakar, “Automatic Fingerprint Matching,” Ph.D. dissertation, Michigan State University, Lansing, MI, United States, 2001.

[7] L. Hong, “Automatic Personal Identification Using Fingerprint,” Ph.D. dissertation, Michigan State University, Lansing, MI, United States, 1998.

[8] H.B. Kekre and V.A. Bharadi, “Fingerprint & Palmprint Segmentation by Automatic Thresholding of Gabor Magnitude,” *presented at Second International Conference on Emerging Trends in Engineering and Technology*, 2009.

[9] “The History of Fingerprints,” [Online]. Available: http:/withww.onin.com/fp/fphistory.html [Accessed: Aug. 23, 2010].

[10] W. Badler, “Dermatoglyphics,” *Science Transition*, vol. 9, pp 95, 1991.

[11] M. Kuchen and C. Newell, “A Model for Fingerprint Formation,” *Europhysletters*, vol. 68, no. 1, pp. 141-147, 2004.

[12] S.S.R. Malalur, “A Pseudo-Spectral Fusion Approach for Fingerprint Matching,” M.S. thesis, The University of Texas at Arlington, Arlington, TX, United States, 2004.

[13] L. Hong and A.K. Jain, “Fingerprint Image Enhancement: Algorithm and Performance Evaluation”, *IEEE Transaction on Pattern Analysis and Machine Intelligence*, vol. 20, no. 8, August 1998.

[14] P. Ramo, M. Tico, V. Onnia and J. Saarinen, “Optimized Singular Point Detection Algorithm for Fingerprint Images,” *proceedings of International Conference on Images Processing*, vol. 3, pp. 242-245, 2001.

[15] A. Ross, A.K. Jain and J. Reisman, “A Hybrid Fingerprint Matcher”, *Pattern Recognition*, vol. 36, no. 7, pp. 1661-1673, 2003.

[16] A. Ross, A.K. Jain and J. Reisman, “A Hybrid Fingerprint Matcher”, *Proc. Of International Conference on Pattern Recognition*, vol. 3, pp. 795-798, Quebec City, August 11-15, 2002.

[17] D. Maltoni, D. Maio, A.K. Jain and S. Prabhakar, “Handbook of Fingerprint Recognition”. Springer, 2003.

[18] N. Ratha and R. Bolle, Eds., “Automatic Fingerprint Recognition Systems”. Springer, 2004.

[19] A.K. Jain, “Fundamentals of Digital Image Processing”, Prentice-Hall, 1989.

[20] H.C. Lee and R.E. Gaensslen, Eds., “Advanced in Fingerprint Technology”, CRC Press, 2001.

[21] B.G. Sherlock and D.M. Monro, “A Model for Interpreting Fingerprint Topology,” *Pattern Recognition*, vol. 26, no. 7, pp. 1047-1055, 1993.

[22] Z. Kovacs-Vajna, R. Rovatti and M. Frazzoni, “Fingerprint Ridge Distance Computation Methodologies”, *Pattern Recognition*, vol. 33, pp. 69-80, 2000.

[23] J.C. Russ, “The Image Processing Handbook”, CRC Press, Inc., 1992.

[24] K.R. Rao, D.N. Kim and J.J. Hwang, “Fast Fourier Transform – Algorithms and Applications”, Springer, 2010.

[25] C. Yu, M. Xie and J. Qi, “An Effective and Robust Fingerprint Enhancement Method,” *presented at 2008 International Symposium on Computational Intelligence and Design*, 2008.

[26] M.S. Helfroush, “Non-Minutiae Based Fingerprint Verification,” Ph.D. Thesis, Tarbiat Modares University, Tehran, Iran, 2006.

[27] “Fingerprint Verification Competition 2000,” [Online]. Available: http://bias.csr.unibo.it/fvc2000 [Accessed: Sept. 10, 2010].

[28] D. Maio, D. Maltoni, R. Cappelli, J.L. Wayman and A.K. Jain, “FVC2000: Fingerprint Verification Competition,” Biometric System Lab (BIOLAB)-DEIS and U.S. National Biometric Test Center, College of Engineering and Pattern Recognition and Image Processing Laboratory, Tech. Rep., 2000.

BIOGRAPHICAL INFORMATION

Michael J. Futer was born in 1980 in Lancaster County, Pennsylvania, United States. He graduated from The Pennsylvania State University in August 2003 with a Bachelor of Science degree in Electrical Engineering and a Business/Liberal Arts minor. He also earned a Master of Science degree in Electrical Engineering from The University of Texas at Arlington in December 2010. His research interests include digital signal and image processing, biometrics and embedded microprocessors. He is currently employed as an electrical engineer in the United States government defense industry and has worked on programs such as U.S. Navy's AN/ARC 209A/B digital FM radio, DARPA's Future Combat Systems NLOS-LS missiles and U.S. Army's Missile Defense Systems PAC-3 Missile and PAC-3 MSE. More recently, he has been involved in programs that include U.S. Army's Thermal Weapon Sight, Driver's Vision Enhancer and Digitally-Enhanced Night Vision Goggle. He also worked on satellite communication systems for the commercial airline industry. He plans to continue on his career path as an electrical engineer in the U.S. government defense industry while exploring part-time software consulting opportunities in the field of biometrics.